Fenton, J. W., II, Olson, T. A., Zabinski, M. P., & Wilner, G. D. (1988) *Biochemistry 27*, 7106-7112.
Francis, C. W., & Marder, V. J. (1986) *J. Lab. Clin. Med. 107*, 342-352.
Francis, C. W., Markham, R. E., Jr., Barlow, G. H., Florack, T. M., Dolrzynski, D. M., & Marder, V. J. (1983) *J. Lab. Clin. Med. 102*, 220-230.
Galanakis, D. K., Lane, B. P., & Simon, S. R. (1987) *Biochemistry 26*, 2389-2400.
Garcia, J. G. N., Siflinger-Birnboim, A., Bizios, R., Del Vecchio, P. J., Fenton, J. W., II, & Malik, A. B. (1986) *Am. J. Physiol. 128*, 96-104.
Glenn, K. C., Carney, D. H., Fenton, J. W., II, & Cunningham, D. D. (1980) *J. Biol. Chem. 255*, 6609-6616.
Hofsteenge, J., Braum, P. J., & Stone, S. R. (1988) *Biochemistry 27*, 2144-2151.
Irwin, D. M., Robertson, K. A., & MacGillivray, R. T. A. (1988) *J. Mol. Biol. 200*, 31-45.
Kawabata, S., Morita, T. Y., Iwanaga, S., & Igaraski, H. (1985) *J. Biochem. 97*, 325-331.
Landis, B. H., Koehler, K. A., & Fenton, J. W., II (1981) *J. Biol. Chem. 256*, 4604-4610.
Levin, E. G., Stern, D. M., Nawroth, P. P., Marlar, R. A., Fair, D. S., Fenton, J. W., II, & Harker, L. A. (1986) *Thromb. Haemostasis 56*, 115-119.
Liu, C. Y., Nossel, H. L., & Kaplan, K. L. (1979) *J. Biol. Chem. 254*, 10421-10425.
Malik, A. B. (1986) *Semin. Thromb. Hemostasis 12*, 184-196.
Martodam, R. R., Baugh, R. J., Twimassi, D. Y., & Liener, I. E. (1979) *Prep. Biochem. 9*, 15-31.
Perdue, J. F., Lubenskyi, W., Kivity, E., Sonder, S. A., & Fenton, J. W., II (1981) *J. Biol. Chem. 256*, 2767-2776.
Powers, J. C., Gupton, B. F., Harley, A. D., Nishino, N., & Whitley, R. J. (1977) *Biochim. Biophys. Acta 485*, 156-166.
Sonder, S. A., & Fenton, J. W., II (1986) *Clin. Chem. (Winston-Salem, N.C.) 32*, 934-937.
Walz, D. A., Anderson, G. F., Ciaglowski, R. E., Aiken, M., & Fenton, J. W., II (1985) *Proc. Soc. Exp. Biol. Med. 180*, 518-526.
Walz, D. A., Wider, M. D., Snow, J. W., Dass, C., & Desiderio, D. M. (1988) *J. Biol. Chem. 263*, 14189-14195.
Wilner, G. D., Danitz, M. P., Mudd, M. S., Hsieh, K.-H., & Fenton, J. W., II (1981) *J. Lab. Clin. Med. 97*, 403-411.
Witting, J. I., Miller, T. M., & Fenton, J. W., II (1987) *Thromb. Res. 46*, 567-574.
Witting, J. I., Pouliott, C., Catalfamo, J. L., Fareed, J., & Fenton, J. W., II (1988) *Thromb. Res. 50*, 461-468.

Complete Resonance Assignment for the Polypeptide Backbone of Interleukin 1β Using Three-Dimensional Heteronuclear NMR Spectroscopy†

Paul C. Driscoll,‡ G. Marius Clore,*,‡ Dominique Marion,‡,§ Paul T. Wingfield,‖,⊥ and Angela M. Gronenborn*,‡
Laboratory of Chemical Physics, Building 2, National Institute of Diabetes, Digestive and Kidney Diseases, National Institutes of Health, Bethesda, Maryland 20892, and Glaxo Institute for Molecular Biology SA, 46 Rue des Acacias, CH-1211 Geneva, Switzerland

Received October 3, 1989; Revised Manuscript Received December 6, 1989

ABSTRACT: The complete sequence-specific assignment of the ^{15}N and ^{1}H backbone resonances of the NMR spectrum of recombinant human interleukin 1β (153 residues, M_r = 17 400) has been obtained by using primarily ^{15}N-^{1}H heteronuclear three-dimensional (3D) NMR techniques in combination with ^{15}N-^{1}H heteronuclear and ^{1}H homonuclear two-dimensional NMR. The fingerprint region of the spectrum was analyzed by using a combination of 3D heteronuclear ^{1}H Hartmann-Hahn ^{15}N-^{1}H multiple quantum coherence (3D HOHAHA-HMQC) and 3D heteronuclear ^{1}H nuclear Overhauser ^{15}N-^{1}H multiple quantum coherence (3D NOESY-HMQC) spectroscopies. We show that the problems of amide NH and C$^{\alpha}$H chemical shift degeneracy that are prevalent for proteins of this size are readily overcome by using the 3D heteronuclear NMR technique. A doubling of some peaks in the spectrum was found to be due to N-terminal heterogeneity of the ^{15}N-labeled protein, corresponding to a mixture of wild-type and des-Ala-1-interleukin 1β. The complete list of ^{15}N and ^{1}H assignments is given for all the amide NH and C$^{\alpha}$H resonances of all non-proline residues, as well as the ^{1}H assignments for some of the amino acid side chains. This first example of the sequence-specific assignment of a protein using heteronuclear 3D NMR provides a basis for further conformational and dynamic studies of interleukin 1β.

Interleukin 1 (IL-1)[1] is a cytokine protein with a variety of pleiotropic effects, interacting with virtually every organ and tissue system in the body, which is secreted from many nucleated cell types, particularly activated monocytes and macrophages. Specific activities identified for IL-1 include thymocyte proliferation via the induction of interleukin 2 release, stimulation of B-lymphocyte proliferation, prostaglandin and collagenase release, induction of acute-phase protein synthesis by hepatocytes, and fibroblast growth factor activity.

† This work was supported by the Intramural AIDS Targeted Antiviral Program of the Office of the Director of the National Institutes of Health (to G.M.C. and A.M.G.).
‡ National Institutes of Health.
§ Present addresses: Centre de Biophysique Moléculaire, CRNS 1A, Avenue de la Recherche Scientifique, 45071 Orléans Cedex 2, France.
‖ Glaxo Institute for Molecular Biology SA.
⊥ Present address: Protein Expression Laboratory, Building 6B, National Institutes of Health, Bethesda, MD 20892.

[1] Abbreviations: IL-1, interleukin 1; IL-1α, interleukin 1α; IL-1β, interleukin 1β; NMR, nuclear magnetic resonance; NOE, nuclear Overhauser effect; NOESY, nuclear Overhauser effect spectroscopy; HOHAHA, homonuclear Hartmann-Hahn spectroscopy; HMQC, heteronuclear multiple quantum coherence spectroscopy; COSY, correlated spectroscopy; P.COSY, primitive COSY; $d_{XY}(i,i+1)$, NOE between proton X on residue i and proton Y on residue i + 1.

0006-2960/90/0429-3542$02.50/0

The physiological effects of IL-1 are thus central to the immune and inflammatory responses [see Dinarello (1984, 1988), Oppenheim et al. (1986), and Moore (1989) for reviews]. From a pharmacological point of view IL-1 is found to be cytocidal for certain tumor target cells (Onozaki et al., 1985) and appears to be a potent hyperalgesic (Ferreira et al., 1988). Two distinct coding sequences have been cloned that show essentially identical IL-1 activity (Auron et al., 1984; March et al., 1985). They are known as interleukin 1α (IL-1α) and interleukin 1β (IL-1β). The proteins have similar molecular weights (18 000 and 17 400, respectively), but possess only 25% sequence homology, yet they are found to compete for the same IL-1 receptor (Lowenthal & MacDonald, 1986; Kilian et al., 1986; Dower et al., 1986; Matsushima et al., 1986; Wingfield et al., 1986, 1987a). In both cases the gene encodes for a 31-kDa precursor that is processed to the mature form by a coinduced convertase (Kostura et al., 1989). In the case of IL-1α the preprotein displays full activity, while the pre-IL-1β is inactive. IL-1β is the predominant IL-1 protein found in the extracellular environment, and there is some evidence to suggest that IL-1α activity is mostly associated with the cell membrane (Dinarello, 1988; Fuhlbrigge et al., 1988). Recently a few differences have been found in the biological properties of these two molecules, and it has been suggested that T and B cells possess structurally different IL-1 receptors with distinct binding properties for IL-1α and IL-1β (Scapigliatti et al., 1989). The molecular basis for the similarity of the physiological effects of these two proteins is poorly understood. A preliminary model of the structure of the mature form of IL-1β from low-resolution (3 Å) X-ray diffraction studies has appeared in the literature (Priestle et al., 1988), but no coordinates are yet available.[2] As part of an ongoing program designed to elucidate structure–function relationships for these proteins (Gronenborn et al., 1986, 1988; MacDonald et al., 1986; Wingfield et al., 1987b,c, 1989), we have been engaged in the application of nuclear magnetic resonance spectroscopy (NMR) to studies of their conformation. In this paper we present the complete assignment of the polypeptide backbone resonances of recombinant human IL-1β using mainly three-dimensional heteronuclear NMR.

The application of two-dimensional (2D) NMR spectroscopy to the study of the structure of small proteins (M_r < 10 000) is now well established (Wüthrich, 1986; Clore & Gronenborn, 1987, 1989). There are a number of obstacles to the extension of 2D NMR methods to proteins with molecular weights much greater than 10 000. First, the increasing number of resonances in the spectrum leads to greater overlap and chemical shift degeneracy in the 2D spectrum, increasing the complexity of the spectrum to a point where its analysis becomes overly difficult, if not impossible. Second, the intrinsic property of the nuclear transverse relaxation time T_2 decreases with increasing molecular weight. This leads to a general reduction in the ability to trace out through-bond connections via ^1H–^1H scalar coupling, a fundamental requirement for the sequence-specific assignment process.

Two separate approaches have been taken to increase the scope of the NMR method. Three-dimensional (3D) homonuclear ^1H NMR has been successfully shown to increase the resolution of the traditional 2D NMR spectrum of proteins (Oschkinat et al., 1988, 1989a,b; Vuister et al., 1988). However, since one of the magnetization-transfer steps in these experiments depends on ^1H–^1H scalar couplings, they suffer from the concurrent loss of sensitivity that is observed in the 2D *J*-correlated spectra of large proteins. Indeed, no example of the applications of homonuclear 3D methods has yet been successfully applied to a molecule the size of I1-1β. In the case of recombinant proteins produced by overexpression of the gene in bacterial or other cell systems, a number of superior options become available. These are based on the replacement of ^1H by NMR-inactive ^2H (LeMaster & Richards, 1988; Torchia et al., 1988a) or the inclusion of NMR-active heteronuclei, such as ^{13}C and ^{15}N, by random (Clore et al., 1988; Stockman et al., 1988; Gronenborn et al., 1989a, 1990) or amino acid specific isotope labeling (McIntosh et al., 1987a,b; Torchia et al., 1988b, 1989). Various combinations of amino acid specific ^2H, ^{13}C, and ^{15}N labeling have been used to aid the complete assignment of the backbone resonances of staphylococcal nuclease (18 kDa; Torchia et al., 1989). The application of selective isotope labeling is in general laborious as many different labeled samples must be prepared under the same conditions to complete the assignment task. Random ^{13}C and ^{15}N labeling opens up the possibility of a number of heteronuclear 2D NMR techniques which, because of the altered chemical shift dispersion of the spectrum of the heteronucleus, provide an opportunity of resolving ambiguities present in the 2D ^1H spectrum (Clore et al., 1988; Gronenborn et al., 1989a, 1990; Forman-Kay, 1990). More importantly, the use of the heteronuclear chemical shift as the third dimension in heteronuclear 3D NMR experiments gives rise to spectra in which resonance overlap is greatly reduced (Marion et al., 1989a,b; Fesik & Zuiderweg, 1988; Zuiderweg & Fesik, 1989). Compared to purely homonuclear ^1H 3D NMR spectroscopy, sensitivity is essentially completely retained because of the efficient transfer of magnetization from the heteronucleus to the directly bonded proton. Moreover, we have previously indicated that the combination of 3D heteronuclear ^1H Hartmann–Hahn ^{15}N-^1H multiple quantum coherence (3D HOHAHA–HMQC) and 3D heteronuclear ^1H nuclear Overhauser ^{15}N–^1H multiple quantum coherence (3D NOESY–HMQC) spectroscopies provides a good basis for the assignment of the spectrum of a predominantly β-sheet protein such as IL-1β (Marion et al., 1989b). In this paper we extend the results reported earlier. The complete assignment of the backbone resonances of this protein is presented, and the specific advantages of the 3D heteronuclear NMR experiments in an application to a large protein are demonstrated. To our knowledge this represents the first protein for which the complete backbone assignment has been accomplished by using 3D NMR techniques.

Experimental Procedures

Interleukin 1β Preparation and ^{15}N Labeling. Recombinant IL-1β was prepared by using *Escherichia coli* harboring the expression vector derived from pPLc24 (Buell et al., 1985) in which IL-1β is expressed under the control of the bacteriophage λ P_L promoter and the ribosome binding site of the bacteriophage Mu *ner* gene (Wingfield et al., 1986). Uniform ^{15}N labeling to a level of >95% was obtained by growing the cells in minimal medium with $^{15}NH_4Cl$ as the sole nitrogen source. The proteins were purified as described previously (Wingfield et al., 1986).

Mutagenesis of IL-1β. Site-specific mutants were constructed by oligonucleotide-directed mutagenesis using the

[2] Added in proof: Since the submission and acceptance of this paper, two reports on the refined X-ray structure of IL-1β at 2-Å resolution have appeared in the literature [Finzel, B. C., Clancy, L. L., Holland, D. R., Muchmore, S. W., Watenpaugh, K. D., & Einspahr, H. M. (1989) *J. Mol. Biol. 209*, 779–791; Priestle, J. P., Schär, H.-P., & Grütter, M. G. (1989) *Proc. Natl. Acad. Sci. U.S.A. 86*, 9667–9671]. The results presented in this paper, as well as in the subsequent paper (Driscoll et al., 1990) on the secondary structure analysis and molecular topology of IL-1β, are in complete agreement with the high-resolution X-ray data.

two-primer approach (Norris et al., 1983; Zoller & Smith, 1984) as described previously (Gronenborn et al., 1986). The A1C mutant was used together with the wild-type protein in the sequence-specific assignment procedure, while the following point mutant IL-1β molecules were utilized in the confirmation of the complete sequential assignment of the spectrum of the wild-type molecule: K27C, K93A, K94A, and C71S.

N-Terminal Sequencing. N-Terminal amino acid sequence determination was performed by automated Edman degradation with a gas-phase sequencer (Applied Biosystems Model 470A). The results indicated that ^{15}N-labeled wild type IL-1β produced in *E. coli* with minimal medium comprised two species, 60% with N-terminal Ala-1 and 40% N-terminal Pro-2. For the ^{15}N-labeled A1C mutant IL-1β produced in minimal medium, the N-terminal sequencing indicated that the protein was completely missing the Cys-1 residue, being 100% *N*-Pro-2. This protein product of the A1C mutant construct is therefore referred to here as des-Ala-1-IL-1β. Unlabeled IL-1β samples (wild type and point mutants) were produced from *E. coli* grown in full medium. These comprised mixtures of *N*-Met- and *N*-[Ala-1]-IL-1β proteins, due to the incomplete processing of the initiating methionine (Wingfield et al., 1987c).

NMR Sample Preparation. The buffer for all NMR experiments was 100 mM, pH 5.4, sodium acetate-d_3 (95% H_2O/5% D_2O) containing the various proteins at a concentration of ~2.3 mM. The sample temperature during the 3D NMR experiments was 36 °C.

NMR Spectroscopy. All NMR spectra were recorded on a Bruker AM600 spectrometer, operating entirely in the reverse mode. Thus, all ^{1}H pulses were generated by using the decoupler channel, while ^{15}N pulses were produced by suitable amplification of pulses generated from the low-power observe channel. The spectrometer was also equipped with digital phase shifters, fast switching of the ^{1}H decoupler and ^{15}N observe power levels, and a hard-wired facility for X-nucleus decoupling using the GARP (Shaka et al., 1985) composite pulse decoupling sequence.

The following 2D spectra were recorded in D_2O solution: 100-ms NOESY (Jeener et al., 1979; Macura et al., 1981) at 27 and 36 °C; 40-ms HOHAHA (Braunschweiler & Ernst, 1983; Davis & Bax, 1985) at 27 and 36 °C; and P.COSY (Mueller, 1987; Marion & Bax, 1988) at 36 °C. Very low power phase locked presaturation of the residual HOD signal was employed. 2D HOHAHA and NOESY spectra in H_2O solution were recorded with a jump-and-return read pulse as described previously (Bax et al., 1987; Driscoll et al., 1989). 2D COSY (Aue et al., 1976) spectra were recorded in H_2O by using phase-locked presaturation, and the SCUBA technique was utilized for the recovery of fingerprint region cross-peaks with C$^\alpha$H chemical shifts coincident with the solvent H_2O resonance (Brown et al., 1987). The sweepwidth employed was 8.4 kHz in each dimension. 2K data points were recorded in F_2 with 800–900 increments in F_1. Typically, 16–32 scans were collected per t_1 increment with a relaxation delay of 1.5–1.7 s. Where these experiments were applied to ^{15}N-labeled protein, ^{15}N decoupling was achieved by gating on the GARP unit during the t_1 evolution and detection periods.

For inverse ^{15}N–^{1}H correlation experiments, a double INEPT transfer scheme, otherwise known as the "Overbodenhausen" experiment (Bodenhausen & Ruben, 1980; Bax et al., 1990a; Kay et al., 1989b), was used. The ^{15}N–^{1}H J coupling evolution and refocusing delays of the INEPT portions of the pulse sequence were set to 2.3 ms [slightly shorter than $1/(4J_{NH})$]. Off-resonance DANTE-style presaturation of the H_2O signal was used to suppress the water resonance (Kay et al., 1989a). A sweepwidth of 4.2 kHz was employed (H_2O signal at right-hand edge of the spectrum), with a 1K block size in F_2 and 512 increments in F_1. The sweepwidth in F_1 was 3.3 kHz with an offset of 121 ppm from liquid ammonia (this causes the folding of two arginine side-chain N$^\epsilon$H signals into regions of the spectrum devoid of other signals).

All the 2D experiments were recorded by using time-proportional phase incrementation (TPPI) for quadrature detection (Ernst et al., 1987) and were acquired in the phase-sensitive mode as described by Marion and Wüthrich (1983).

The heteronuclear 3D HOHAHA–HMQC and NOESY–HMQC experiments were recorded in a manner that maximizes the digital resolution in all three dimensions (Kay et al., 1989a). A complete description of the pulse sequences is given in our previous paper (Marion et al., 1989b) and is therefore only summarized below. The 3D NOESY–HMQC sequence is given by

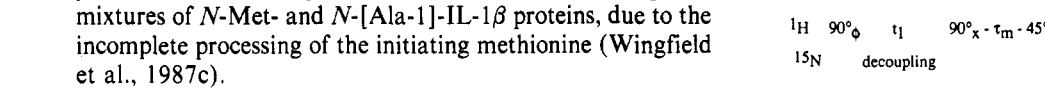

while the 3D HOHAHA–HMQC sequence is given by

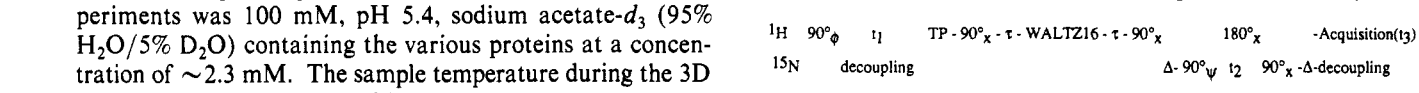

The phase cycling to obtain pure-phase absorption spectra by the method of States et al. (1982) is the same for both experiments and is given by $\phi = x,y,-x,-y$, $\psi = 4(x),4(-x)$, and Acquisition = $2(x),4(-x),2(x)$, with data for odd- and even-numbered scans stored separately. For quadrature detection in F_2 the sequence is repeated with the phase ψ incremented by 90°. The 90° ^{1}H pulse was 13.5 μs for the 3D NOESY–HMQC and 28.5 μs for the 3D HOHAHA–HMQC; the 90° ^{15}N high-power pulse was 73 μs, and the lower power 90° ^{15}N pulse used for GARP decoupling was 250 μs. The ^{15}N–^{1}H coupling and evolution time Δ in both experiments was set to 4.5 ms, slightly less than $1/(2J_{NH})$. The $45°_x$–τ–$45°_x$ off-resonance 1–1 read pulse in the 3D NOESY–HMQC experiment is used to help suppress the residual H_2O magnetization at the end of the NOESY mixing time and allows the power of the presaturation pulse train to be minimized; the delay τ between the two 45° pulses was set to 203 μs with the carrier placed 2083.3 Hz downfield of the water resonance. The trim pulse (TP) in the 3D HOHAHA–HMQC experiment was set to 1.5 ms, and the fixed delays (τ = 7.5 ms = mixing time/4) immediately before and after the WALTZ16 pulse train were used to remove rotating frame NOE effects. The latter delays also provide time to switch the transmitter offset for the mixing sequence to a frequency that maximizes the efficiency of the HOHAHA magnetization transfer between the NH and C$^\alpha$H protons, namely, to 6 ppm (~1.3 ppm downfield of the water resonance). Between scans, off-resonance DANTE-style presaturation of the H_2O signal with a very weak radio frequency field of 10–15 Hz was applied for 1.5 s to suppress the water resonance.

Both 3D HOHAHA–HMQC and NOESY–HMQC experiments were recorded on a Bruker AM600 NMR spectrometer. The two experiments were recorded consecutively on the same sample to minimize any differences in both the sample and recording conditions. The mixing times were 30 ms for the 3D HOHAHA–HMQC and 100 ms for the 3D NOESY–HMQC experiments. For both experiments the F_3 and F_2 sweepwidths were 4166.7 and 1580.8 Hz (corre-

sponding to 26 ppm in the ^{15}N dimension), respectively. Since it is not necessary to record those regions of the spectrum in F_1 for which no cross-peaks are observed, these can be folded in the 3D spectrum without introducing confusion. Thus, in the 2D HOHAHA experiment no cross-peaks are observed from an amide NH to any of the high-field aliphatic groups in F_1 (see Figure 1A). In the 3D HOHAHA–HMQC experiment we therefore kept the F_1 sweepwidth to only 6060 Hz (10.1 ppm). In the 3D NOESY–HMQC experiment, where NOEs from NH groups to high-field aliphatic groups can be observed, we increased the F_1 sweepwidth to 6784 Hz (11.3 ppm). In neither case did we fold low-field NH signals into the aliphatic region in F_1 (though this may be desirable—especially in the 3D HOHAHA–HMQC spectrum). Because the carrier offset was set to the center of the amide NH region of the ^1H spectrum in F_3, shifting of the carrier in the F_1 dimension was required. This was achieved by applying a linear phase correction to the time domain data in t_1 during the processing stage. In the 3D HOHAHA–HMQC experiment we employed a shift of the carrier position upfield from 8.1 to 6.0 ppm during the WALTZ spin-lock period. This is readily accomplished during the delays bracketing the spin-lock sequence that are used to compensate for rotating frame NOE effects (set to 7.5 ms each). This procedure maximizes the efficiency of the Hartmann–Hahn magnetization transfer between the amide and $C^\alpha H$ protons. Quadrature detection in the F_1 and F_2 dimensions was obtained by using the method of States et al. (1982). In each case 128 complex t_1, 32 complex t_2, and 512 real t_3 data points were recorded with acquisition times of 21.12 (t_1, HOHAHA), 18.87 (t_1, NOESY), 20.24 (t_2), and 61.44 ms (t_3).

Data Processing. All 2D NMR experiments were processed by using the Bruker DISNMR software on an ASPECT 1000 datastation. The 3D NMR experiments were processed on a SUN 4 computer using a simple in-house-written routine for the F_2 Fourier transform, together with the commercially available 2D software package NMR2 (New Methods Research Inc., Syracuse, NY) for processing of the F_1–F_3 planes, as described previously (Kay et al., 1989a). Zero-filling (once in each dimension) was employed to yield a final absorptive spectrum of 256 × 64 × 512 data points. The weighting function applied in the F_1 and F_3 dimensions was a singly shifted 60° sine bell window function, while a doubly shifted sine bell function, shifted by 60° at the beginning of the window and by 10° at the end, was used in the F_2 dimension (Kay et al., 1989a). As a result the apodization function does not have a value of zero at the end of the time domain data in t_2. This avoids too low a weighting factor for the last t_2 increments, thereby improving sensitivity and resolution. In the case of t_2 data comprising 32 complex points, this is implemented by applying a singly shifted 60° sine bell function over 34 complex points. A linear frequency domain base-line correction was applied in F_3 prior to Fourier transformation in F_1. Noninteractive phase correction in the F_1 and F_2 dimensions was applied according to the formulas given previously (Kay et al., 1989a; Marion et al., 1989b). The digital resolution in the final 3D spectrum was 8.13 Hz/point in F_3, 24.7 Hz/point in F_2, and 23.6 Hz/point in F_1 (HOHAHA) and 26.5 Hz/point in F_1 (NOESY). Plots of the 3D spectra were produced by using a simple contouring algorithm, to produce POSTSCRIPT files that were output to a laser printer.

Results

Figure 1 shows the amide NH–aliphatic regions of the ^1H 2D NOESY (mixing time 100 ms) and 2D HOHAHA (mixing time 40 ms) spectra of wild-type recombinant IL-1β,

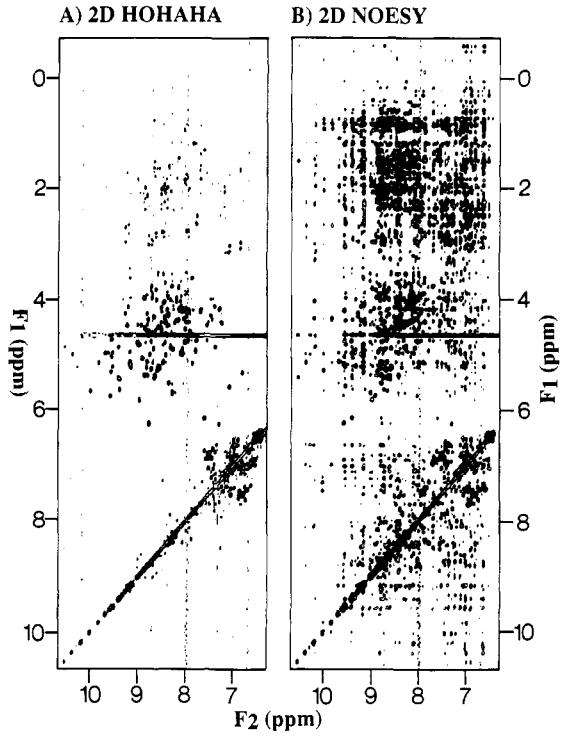

FIGURE 1: Amide (F_2 axis)–aliphatic (F_1 axis) regions of (A) ^1H 2D HOHAHA and (B) 2D NOESY spectra of interleukin 1β recorded at 600 MHz, 36 °C and pH 5.4, 100 mM sodium acetate-d_3 (95% H_2O/5% D_2O). The spectra were recorded with a jump and return read pulse, with mixing times of 39 and 100 ms, respectively.

obtained at pH 5.4 and 36 °C. It is clear from these spectra that while there are many resolved cross-peaks in some regions of the spectrum, there is also extensive cross-peak overlap and chemical shift degeneracy. When the sequence-specific assignment of a protein spectrum is made, variation of temperature and pH is often used to overcome such problems. The use of a point mutation in the amino acid sequence of the protein can also be of assistance in this regard, providing it does not significantly alter the overall structure (Gronenborn et al., 1986). In the case of IL-1β, however, extensive analysis of the 2D spectra using all these protocols yielded "hard" assignments for only a small number (around 30%) of amino acid residues. We therefore turned to novel heteronuclear experiments, particularly 3D NMR, to undertake the assignment task.

The basis for the ^{15}N–^1H heteronuclear 3D experiments lies in editing the ^1H 2D spectrum according to the chemical shift of the directly bonded amide ^{15}N nucleus. This information is contained in the ^{15}N–^1H reverse-correlation spectrum, which corresponds to the F_2–F_3 projection of the 3D spectrum. The 3D experiments we have used are based on the HMQC pulse sequence in combination with various ^1H 2D sequences. For routine examination of the 2D ^{15}N–^1H correlation spectrum, however, the Overbodenhausen experiment provides superior resolution in the ^{15}N dimension compared with that of the HMQC experiment (Bax et al., 1990a). Figure 2 shows the Overbodenhausen inverse ^{15}N–^1H correlation spectrum of a randomly ^{15}N labeled sample of wild-type recombinant IL-1β, obtained under the same conditions as for the 2D spectra shown in Figure 1, together with the assignments that were obtained as a result of the investigation reported in this paper. For the most part the cross-peaks in this spectrum are well resolved. By careful analysis of this and similar spectra obtained under slightly different conditions of pH and temperature, it was possible to identify 151 individual amide NH peaks. Some of these correlation peaks exhibit a broad line

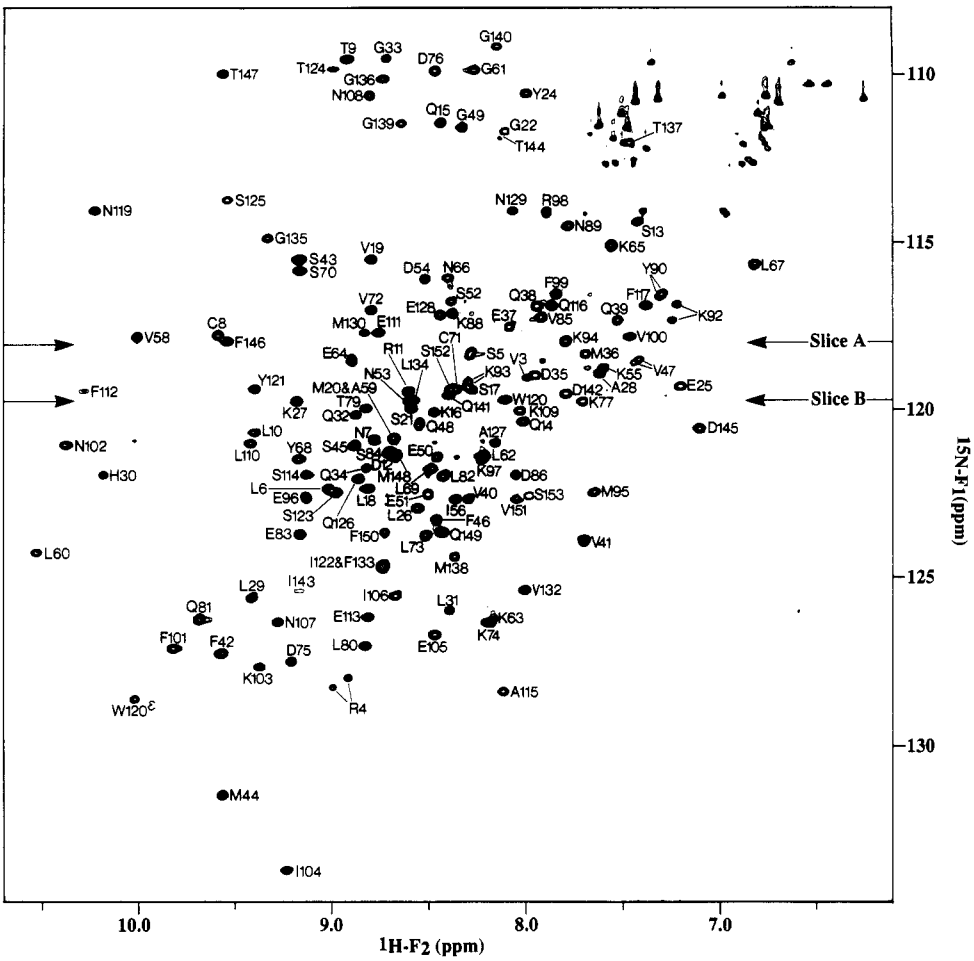

FIGURE 2: ^{15}N–^{1}H Overbodenhausen correlation spectrum of ^{15}N-labeled wild-type interleukin 1β recorded under the same conditions as the spectra in Figure 1. The assignments obtained as described in this paper are indicated. Some residues exhibit two peaks due to the sequence heterogeneity of the N terminus of the protein. Two arrows indicate the ^{15}N chemical shifts for the two slices of the 3D spectra shown in Figure 4.

shape and are only just visible at the contour level used in Figure 2. In many cases this is consistent with the absence of a peak from the 2D ^{1}H COSY spectrum and a broad peak in the 2D ^{1}H HOHAHA spectrum.

IL-1β contains 153 amino acid residues, including 8 prolines. Excluding the N-terminal residue, for which the amino group is generally not observed in protein spectra, one might expect to observe 144 amide signals. The discrepancy in the numbers of predicted and observed peaks indicates either structural and/or conformational heterogeneity in the ^{15}N-labeled wild-type IL-1β sample. The discrepancy was resolved by analysis of the spectrum of a ^{15}N-labeled sample of IL-1β which was lacking the N-terminal residue, Ala-1. This protein was constructed as a point mutant where a cysteine residue was replaced for the N-terminal alanine (i.e., [^{15}N]-A1C-IL-1β). The expressed protein, however, was found by N-terminal amino acid sequencing to start exclusively at Pro-2, the N-terminal cysteine residue having been removed by enzymatic cleavage in *E. coli*. For this des-Ala-1-IL-1β only 143 amide signals were observed in the ^{1}H-^{15}N correlation experiment. N-Terminal amino acid sequencing of the wild-type ^{15}N-labeled protein showed it to be a mixture of two polypeptides, one with the correct N-terminal Ala-1 residue and a minor form beginning at Pro-2 in a ratio of approximately 3:2. In neither case was the sample found to contain any protein containing the initiating methionine (Wingfield et al., 1987c). The analysis of the sequential assignment and protein secondary structure indicated that the extra peaks in the sample of wild-type IL-1β are due to the resolvable difference of the

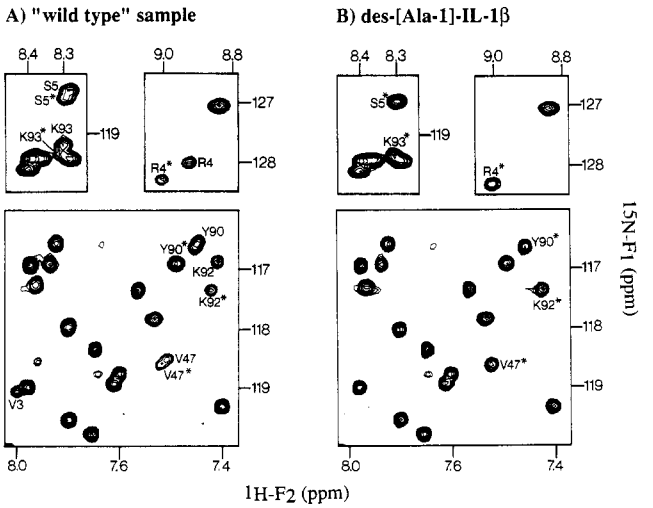

FIGURE 3: Three expanded regions of the ^{15}N–^{1}H Overbodenhausen correlation spectra of ^{15}N-labeled wild-type and des-Ala-1-interleukin 1β. The doubling of a number of peaks in the wild-type spectrum is illustrated. Assignments for those peaks due to the minor des-Ala-1 form are indicated by asterisks. Note the Val-3 cross-peak is only observed in the spectrum of the wild-type sample.

chemical shifts in the two forms of the protein for seven amides (Arg-4, Ser-5, Val-47, Gln-48, Tyr-90, Lys-92, and Lys-93), with one amide (i.e., that of Val-3) only detectable in the spectra of the "normal" Ala-1-containing protein. It should be pointed out that the nature of this heterogeneity was not readily evident from the 2D spectra, until after the analysis

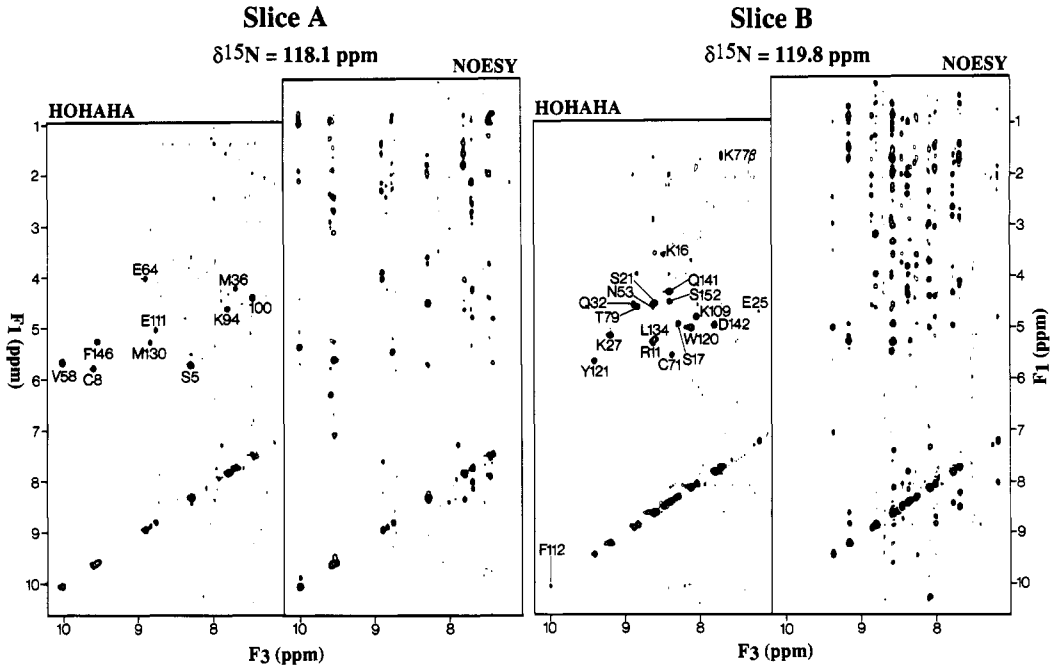

FIGURE 4: Two slices from 3D HOHAHA-HMQC and 3D NOESY-HMQC spectra of wild-type interleukin 1β described in the text. Because the two experiments were recorded by using an identical sweepwidth in F_2, there is a correspondance between the peaks in the HOHAHA slice and the respective slice from the NOESY spectrum. The different sizes of the slices in the F_1 dimension are due to the different F_1 sweepwidths used in the two experiments. Slice A corresponds to the F_1–F_3 cross section of the 3D spectrum at a ^{15}N chemical shift of 118.1 ppm and slice B to a cross section at 119.8 ppm. The assignments of the intraresidue NH–C$^{\alpha}$H correlations are indicated in the respective HOHAHA slices. In slice B the intraresidue NH–C$^{\alpha}$H cross-peak of Lys-77 is lost because of the presaturation of the H_2O resonance; the NH–C$^{\beta}$H cross-peaks are indicated for this residue. The NH–C$^{\alpha}$H cross-peak of Phe-112 is not visible at the contour level chosen (this residue has an exceptionally broad amide proton resonance); the diagonal peak is indicated for this residue.

of the 3D spectra reported below. Figure 3 illustrates small regions of the Overbodenhausen spectra obtained with these two protein samples. The doubling of the cross-peaks that have been attributed to Arg-4, Ser-5, Val-47, Tyr-90, Lys-92, and Lys-93 is indicated. Note that only one peak for Val-3 has been found for the sample containing the wild-type protein. This is absent from the spectrum of des-Ala-1-IL-1β.

Figure 4 shows two representative pairs of slices from the heteronuclear 3D HOHAHA-HMQC and NOESY-HMQC spectra. The two spectra were obtained under precisely the same conditions of temperature and pH. The slices are taken at ^{15}N chemical shifts indicated by the markers in the 2D ^1H–^{15}N correlation spectrum shown in Figure 2. In the first pair of spectra (slice A, $\delta^{15}N$ = 118.0 ppm) there are 10 clearly resolved fingerprint region NH–C$^{\alpha}$H correlations in the HOHAHA slice. All but one of these exhibit discernible NOEs in the NOESY slice. The high sensitivity of the experiments is clearly apparent. It is important, however, to note the absence of relayed NH–C$^{\beta}$H correlations in the HOHAHA slice. The second pair of spectra (slice B, $\delta^{15}N$ = 119.8 ppm) contains the cross-peaks corresponding to 19 different amide protons (the assignments are indicated in the figure; the amide NH of Phe-112 has a relatively broad proton line width and the NH–C$^{\alpha}$H cross-peak is not visible at the contour level chosen). This represents one of the most crowded slices in the whole 3D spectrum of IL-1β. In this case a few relayed NH–C$^{\beta}$H connections can be observed in the HOHAHA slice (Arg-11, Ser-21, Gln-32, Lys-77, Thr-79, Trp-120, Gln-141, and Ser-152). Note that because of the 60° shifted sine bell weighting function, which restricts the resolution enhancement used in processing the ^{15}N F_2 dimension, and the intrinsic ^{15}N multiple quantum line width, almost all the peaks appear in more than one slice of the 3D spectrum. Thus, in the case of slice A in Figure 4, although the sets of peaks arising from 10 amide NH protons are present, only 4 of these sets are at their maximum intensity (Ser-5, Met-36, Lys-94, and Phe-146). All of the remaining six sets of cross-peaks have their maximum intensity in one of the adjacent slices. In slice B of Figure 4, only 7 of the 19 sets of cross-peaks are present at their maximum intensity (Lys-27, Asn-53, Lys-77, Trp-120, Leu-134, Gln-141, and Asp-142). The NH–C$^{\alpha}$H cross-peak of K77 is missing from the HOHAHA slice. This is a consequence of the fact that presaturation of the H_2O resonance is used in the 3D pulse sequences. Thus, these 3D experiments suffer from the problem of bleaching out C$^{\alpha}$H resonances that are degenerate with the strong solvent peak. However, the decoupler power used for the suppression of the solvent peak is minimal. In the whole of the 3D HOHAHA-HMQC spectrum only six NH–C$^{\alpha}$H fingerprint correlations are completely attenuated in this manner (Val-19, His-30, Val-47, Lys-77, Glu-83, and Lys-103). The loss of peaks due to presaturation is less of a problem in our 3D NOESY-HMQC spectrum because a 1–1 selective read pulse at the end of the NOESY portion of the sequence is employed which allows the use of lower power for the presaturation pulses. (In principle, this procedure could also be applied in the 3D HOHAHA-HMQC experiment.)

While the increase in resolution in the 3D spectrum is spectacular compared to the 2D spectra of Figure 1, there is still some amide NH chemical shift degeneracy in the individual slices. For example, in slice B in Figure 4, the cross-peaks from Arg-11 and Asn-53 lie along the same NH chemical shift axis, as do the cross-peaks of Ser-152 and Gln-141. As cross-peaks for each amide NH can be found in more than one slice, analysis of the neighboring slices in the 3D spectrum is sufficient to correlate each cross-peak with a given amide NH. This property of the 3D spectrum is illustrated in Figure 5, which shows a small region of five consecutive slices from both the 3D HOHAHA-HMQC and 3D NOESY-HMQC spectra of IL-1β. The figure shows in

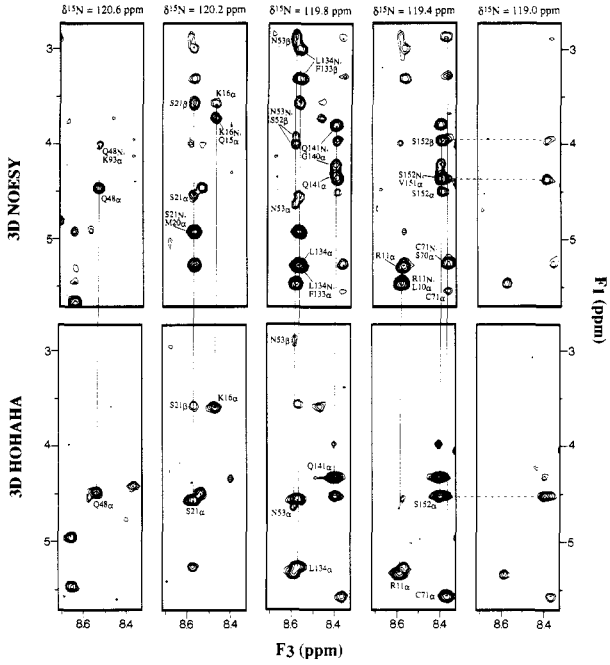

FIGURE 5: Small region of five consecutive slices of the 3D NOESY–HMQC (upper) and 3D HOHAHA–HMQC (lower) spectra of interleukin 1β. For a given amide NH the corresponding cross-peaks appear in more than one slice of the 3D spectrum. By following the change in intensity of the cross-peaks through the slices it is possible to assign each peak to a given signal in the 2D ^{15}N–^{1}H correlation spectrum or a given NH–C$^{\alpha}$H peak in the 3D HOHAHA–HMQC spectrum (indicated by the vertical lines). For example, the rightmost slice contains peaks that arise from Ser-152, but which exhibit their maximum intensity in the preceding slice (horizontal dashed lines), where they are degenerate in F_3 with cross-peaks arising from Gln-141. The spectra indicate that it is possible to distinguish cross-peaks that arise from amide NHs that have virtually (Ser-21 and Asn-53) or completely (Arg-11 and Asn-53, Ser-152 and Gln-141) degenerate amide NH ^{1}H chemical shifts and only slightly different ^{15}N chemical shifts.

which slice the cross-peaks arising from each spin system involved appear at their maximum intensity. The resolution of the cross-peaks belonging to Gln-141 and Ser-152 which display degenerate amide NH chemical shifts is diagrammed. As a general rule we have found that if the amide NH signals are resolvable in the Overbodenhausen experiment (i.e., peaks may be overlapping, but the peak maxima must be resolvable), then it is possible to separate the corresponding cross-peaks in the 3D spectrum, in spite of the relatively poor digital resolution in F_2 (24.7 Hz/point). Note that this is possible despite the intrinsically superior F_1 resolution of the Overbodenhausen experiment compared to the HMQC experiment upon which the 3D experiments depend. Under the particular experimental conditions used for these 3D experiments, there are three cases where pairs of residues exhibit ^{15}N and ^{1}H amide chemical shifts that are insufficiently resolved to allow the separation of the respective NOE cross-peaks. These occur for Ile-122 and Phe-133, Met-20 and Ala-59, and Ser-84 and Asp-12. Fortunately, none of these pairs of residues also displays C$^{\alpha}$H chemical shift degeneracy. Because of their characteristic patterns, the spin systems of Ala-59 and Ser-84 are easily recognized even in the 3D spectrum reported here. The remaining spin systems can be separated either in 2D spectra or in the 3D spectrum recorded previously at pH 7.5 and 27 °C (Marion et al., 1989b).

The format of each 3D spectrum, as recorded here, comprises 64 ^{1}H–^{1}H F_1–F_3 slices, each with the representation of a conventional NOESY spectrum. Handling this amount of data in the traditional manner, by overlaying hard paper plots on a light-box, becomes a difficult and tedious process. We therefore adopted a simple method that dramatically facilitates the analysis. The approach is based on eliminating the empty space that is present in the 3D spectrum and the redundancy that is caused by the fact that a series of cross-peaks from a single amide NH may appear in more than one slice of the 3D spectrum. Thus, since there are a relatively small number of peaks in each slice of the spectrum, much of the three-dimensional space is devoid of peaks and therefore useless for the purposes of analysis. The approach we have taken is based on selecting strips of data from each slice containing cross-peaks arising from each amide NH group. Having identified each individual ^{15}N–^{1}H NH correlation in the 2D Overbodenhausen experiment, the 3D slice for which the corresponding cross-peaks displayed the greatest intensity was ascertained. Then the index of the data point in the F_3 dimension closest to the peak maximum of the NH resonance was noted. Next a strip of data of width 17 points (i.e., the center data point ± 8 data points, corresponding in this case to 138.2 Hz or 0.23 ppm) and containing the complex F_1 sweepwidth was extracted from the relevant slice. The width of each strip was at least twice as wide as the base of the broadest cross-peak. These strips of data were then aligned alongside each other to form one large 2D data set. For the purposes of display we have applied a 17-point unshifted (sine)$^{3/2}$ window function (0–π radians) across each strip of data. This has the effect of removing intensity from the edges of each strip which is irrelevant to the amide in question while leaving the absolute heights of those peaks of interest unaltered (i.e., the center point of the 17 is scaled to unity by the window function). We have found that using a 0.23 ppm strip width combined with the (sine)$^{3/2}$ window causes little or no visible distortion of the peaks of interest within each strip. In this way we were able to reduce all of the useful information of the complete 3D spectrum to a relatively small number of 2D plots. Initially, the ordering of the strips into a large 2D plot is purely arbitrary. Subsequent to the completion of the sequential assignment process, the strips can be reordered to be consistent with the protein amino acid sequence. For convenience, Figures 6 and 7 show amide strips that are correctly ordered according to the primary sequence. [We note in passing that, having dramatically reduced the data size of the 3D spectrum, one can extract those regions of importance and, reverting to the time domain data by inverse Fourier transformation, apply linear prediction algorithms (Gesmar & Led, 1988) or maximum entropy reconstruction (Laue et al., 1985) to improve the quality of the data contained within the regions of interest. In this way, we can potentially remove artifacts that arise in the 3D spectrum from truncation of the data in F_1 due to the small number of time points recorded, as well as increase the effective resolution in the F_1 dimension.]

Sequential assignment of the spectrum proceeded by using the traditional approach of identifying through-bond connected "spin systems" joined by short-range through-space NOE connections (Wüthrich, 1986). First, the positions of the HOHAHA peaks for each amide NH were marked on the NOESY strips (Figure 6). This then removes the need to shuffle the NOESY spectrum with the HOHAHA spectrum in the analysis. We found that one of the strongest NOEs for any given amide NH is invariably the sequential C$^{\alpha}$H(i)–NH(i+1) or NH(i)–NH(i+1) connection [denoted $d_{\alpha N}(i,i+1)$ and $d_{NN}(i,i+1)$, respectively]. Long-range NOEs (*viz.*, interstrand NH–NH or NH–C$^{\alpha}$H connections) are invariably of lower intensity (though it must always be borne in mind, especially in β-sheet secondary structure, that such interstrand

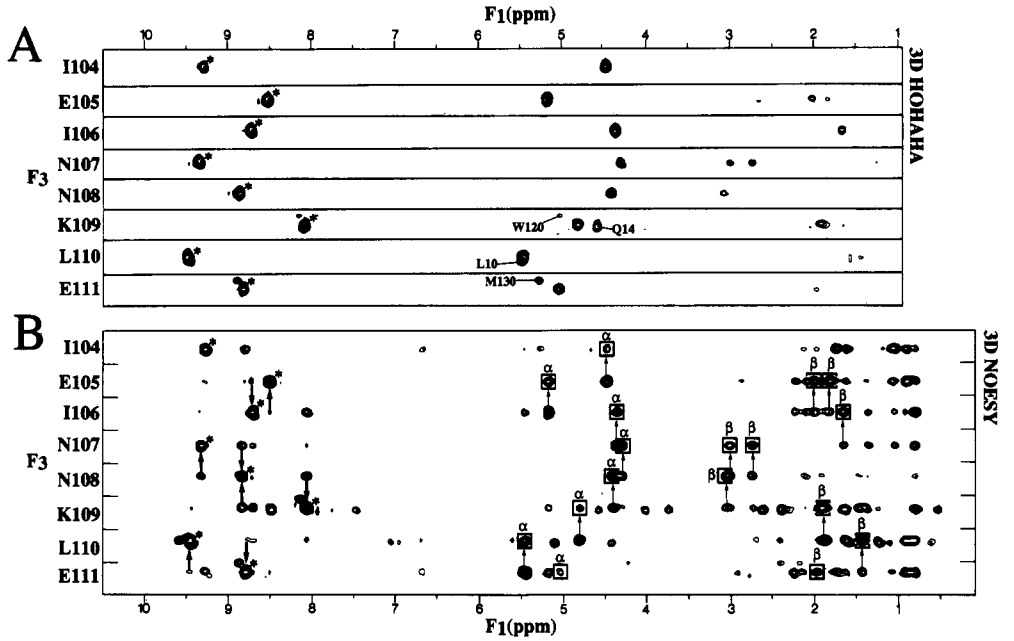

FIGURE 6: (A) Composite of amide strips taken from the 3D HOHAHA–HMQC spectrum of interleukin 1β showing the diagonal NH peaks (labeled with an asterisk), and NH–C$^{\alpha}$H and NH–C$^{\beta}$H cross-peaks for residues Ile-104–Glu-111. Thick horizontal lines separate narrow sections of the slice of the 3D spectrum which contains the cross-peaks of maximum intensity for each residue. In three cases (Lys-109, Leu-110, and Glu-111) additional peaks fall within the narrow strip, as labeled. (B) Corresponding strips from the 3D NOESY–HMQC spectrum of interleukin 1β indicating the NOEs that yield the sequential assignment. Asterisks indicate the position of the diagonal peak for each residue and boxes enclose the intraresidue NH–C$^{\alpha}$H and NH–C$^{\beta}$H cross-peaks that are observed in the corresponding HOHAHA strips. Sequential $d_{NN}(i,i+1)$ NOEs are indicated with thick arrows, sequential $d_{\alpha N}(i,i+1)$ and $d_{\beta N}(i,i+1)$ NOEs with thin arrows. To reduce the complexity, the lines dividing the strips are replaced by tick marks on each side of the figure. The spectra are scaled in the F_3 dimension by a factor of 1.5 with respect to the F_1 dimension. Note that the orientation of the spectra differs by a 90° rotation compared to Figures 4 and 5. The F_3 chemical shifts for Ile-104, Glu-105, Ile-106, Asn-107, Asn-108, Lys-109, Lys-110, and Glu-111 are 9.23, 8.48, 8.67, 9.28, 8.81, 8.03, 9.43, and 8.76 ppm, respectively.

distances can be quite short). In many cases the unambiguous connection of spin systems via a $d_{\alpha N}(i,i+1)$ NOE, where the C$^{\alpha}$H signal has a nondegenerate chemical shift, is a simple matter (Marion et al., 1989b). Also, when two amides are connected by a strong $d_{NN}(i,i+1)$ NOE, this is unequivocally identified as the NOE appears symmetrically about the ^{1}H–^{1}H $F_1 = F_3$ line, with the cross-peak from each side of this line usually in different planes of the 3D spectrum. In fact, there is no case in the spectrum of IL-1β where NH–NH NOEs, short or long range, overlap one another in the 3D spectrum.

Figure 6 illustrates some of these properties of the 3D NMR assignment process for a stretch of the IL-1β protein sequence from Ile-104 to Glu-111. In this representation the amide strips have been ordered according to the polypeptide sequence. The top half of the figure shows the amide strips from the HOHAHA spectrum. On the bottom is the corresponding set of strips from the NOESY spectrum. Note the remarkable absence of cross-peak overlap. A number of sequential NOE connections are indicated by arrows, including $d_{\alpha N}(i,i+1)$ and $d_{NN}(i,i+1)$ NOEs. In a few cases both types of connection can be detected. There are two cases of near chemical shift degeneracy in the example shown that are worth mentioning. In the first case there is a second NH–C$^{\alpha}$H HOHAHA cross-peak with NH chemical shift just upfield of the Lys-109 NH–C$^{\alpha}$H peak. This peak belongs to residue Gln-14. The difference in NH ^{1}H and ^{15}N chemical shifts for these two residues is small (see Figure 2) but sufficient to avoid confusion of the two sets of NOE peaks. In the second case, a similarly small difference in NH chemical shift is found for the amide NHs of Leu-110 and Leu-10. Again the respective NOE peaks are resolvable in the F_3 dimension. This time, however, the two residues exhibit degenerate C$^{\alpha}$H chemical shifts such that the corresponding NH–C$^{\alpha}$H HOHAHA cross-peaks partially overlap and are unresolved in the upper part of the figure. For this section of the protein sequence we can also observe a number of NH–C$^{\beta}$H correlations in the HOHAHA spectrum, which considerably aids the assignment process via the identification of $d_{\beta N}(i,i+1)$ NOEs.

The ^{15}N–^{1}H 3D experiments are specifically designed to overcome the problem of amide NH chemical shift degeneracy in the spectra of large proteins. The presence of C$^{\alpha}$H chemical shift degeneracy in the spectrum can give rise to exactly similar difficulties in the sequential assignment process. This is true even for IL-1β, which, as a β-sheet protein, displays greater overall chemical shift dispersion than an α-helical protein. Indeed, this is a more pernicious problem than amide NH chemical shift degeneracy since the C$^{\alpha}$H chemical shifts are, in general, less sensitive to factors such as temperature and pH. Coupled with the fact that it is necessary to leave the solvent H_2O resonance (and therefore coincident C$^{\alpha}$H resonances) either saturated or unexcited in the NMR experiment, the peaks connecting to C$^{\alpha}$H resonances must be resolved in the F_1 dimension where the intrinsic digital resolution is usually lower than that in the acquisition dimension (F_3). Figure 7 illustrates amide strips taken from the 3D HOHAHA–HMQC (upper) and 3D NOESY–HMQC (lower) spectra for two cases of C$^{\alpha}$H chemical shift degeneracy in the spectrum of IL-1β. The C$^{\alpha}$H resonances of Gln-126 and Glu-64 are degenerate (Figure 7A), as are those of Lys-93 and Ser-13 (Figure 7B). A box in the NOESY strip marks the position of the NH–C$^{\alpha}$H and C$^{\beta}$H HOHAHA correlations observed in the corresponding HOHAHA strip. Only a portion of the aliphatic region of the spectrum in the F_1 dimension is shown. In each example the NOESY strip of the succeeding residue is plotted underneath. The degenerate $d_{\alpha N}(i,i+1)$ NOE connections are indicated by thick arrows.

In the application of the sequential assignment method to proteins of mass <10 kDa, the problem of C$^{\alpha}$H chemical shift

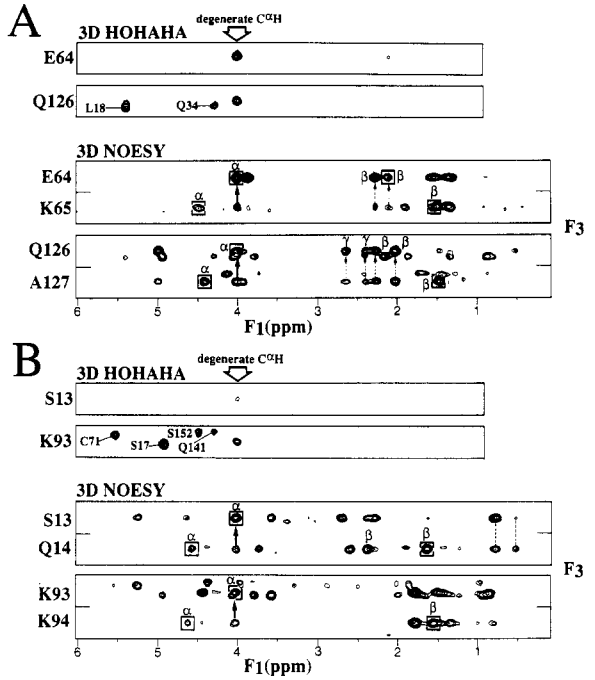

FIGURE 7: Two cases illustrating the resolution of sequential assignments in the case of $C^{\alpha}H$ chemical shift degeneracy, using the 3D spectra of interleukin 1β. (A) Glu-64 and Glu-126 have degenerate $C^{\alpha}H$ chemical shifts as seen from the corresponding amide strips from the 3D HOHAHA–HMQC spectrum (the format here is similar to that of Figure 6, but only the aliphatic region is shown). The sequential assignment between Lys-65 and Glu-64 is obtained by identification of $d_{\alpha N}(i,i+1)$, $d_{NN}(i,i+1)$ (not shown), and $d_{\beta N}(i,i+1)$ NOEs. The sequential assignment between Gln-126 and Ala-127 is obtained from $d_{\alpha N}(i,i+1)$ and $d_{NN}(i,i+1)$ (not shown) NOEs. Dotted lines with arrows indicate $d_{\beta N}(i,i+1)$ and $d_{\gamma N}(i,i+1)$ NOEs that are obtained after identification of $C^{\beta}H$ and $C^{\gamma}H$ chemical shifts from the analysis of correlated spectra in D_2O. (B) Ser-13 and Lys-93 also exhibit degenerate $C^{\alpha}H$ chemical shifts. $d_{\alpha N}(i,i+1)$ and $d_{NN}(i,i+1)$ (not shown) NOEs can be found to connect these residues to Gln-14 and Lys-94, respectively. In neither case, however, has any $d_{\beta N}(i,i+1)$ or $d_{\gamma N}(i,i+1)$ NOE been unambiguously identified. Dotted lines indicate unidentified NOEs that are common to the amide NHs of Ser-13 and Gln-14. This type of effect is observed consistently for pairs of adjacent residues throughout the 3D NOESY–HMQC spectrum of interleukin 1β. The F_3 chemical shifts for Ser-13, Gln-14, Glu-64, Lys-65, Lys-93, Lys-94, Gln-126, and Ala-127 are 7.42, 8.02, 8.90, 7.57, 8.29, 7.80, 8.87, and 8.17 ppm, respectively.

degeneracy is dealt with by identifying secondary sequential NOEs to $C^{\beta}H$ or $C^{\gamma}H$ resonances. For the case of IL-1β, it can be seen in Figure 7 that there is a correlation between the cross-peaks on the axes of the neighboring spin systems for the correct sequential assignments, supported in each case by the identification of a sizeable $d_{NN}(i,i+1)$ NOE (not shown). In the case of the Gln-126/Ala-127 pair, these NOEs can be assigned through analysis of correlated spectra recorded in D_2O, to sequential $d_{\beta N}(i,i+1)$ and $d_{\gamma N}(i,i+1)$ connections. These connections are indicated with broken arrows in Figure 7A. In the case of the Ser-13/Gln-14 pair in Figure 7B, there appear to be common NOEs which, however, cannot be interpreted in terms of short-range connections (dashed lines). Presumably these NOEs are attributable to (as yet unidentified) long-range connections that are common to these neighboring amide NHs in the protein. This correlation of NOE peak positions for adjacent residues, while not proof of the correctness of any given assignment, was observed throughout the spectrum of IL-1β and is clearly evident in both Figures 6 and 7.

A complete analysis of the 3D NOESY–HMQC and 3D HOHAHA–HMQC spectra together with 2D correlated spectra recorded in D_2O solution has enabled the identification of many of the amino acid spin systems for IL-1β. Compared to experience with smaller proteins, the HOHAHA and RELAY–COSY spectra of IL-1β in H_2O solution were poor indicators of the $C^{\beta}H$ chemical shift position, due to the relatively short transverse relaxation times of the amide NH resonances. Thus, in many cases where NH–$C^{\beta}H$ relayed connectivities could not be identified in these spectra, the location of the $C^{\beta}H$ position depended on the correlation of $C^{\alpha}H$–$C^{\beta}H$ cross-peaks in D_2O HOHAHA and P.COSY spectra with intraresidue NH–$C^{\beta}H$ and NH–$C^{\gamma}H$ NOEs in the 3D NOESY spectrum. The considerable degree of $C^{\beta}H$ and $C^{\gamma}H$ resonance overlap makes this difficult for spin systems which extend beyond the β-methylene group. Nevertheless, complete spin system identification was possible for many residues. For example, the fingerprint region cross-peaks of four of the five Ala residues were easily assigned because of the relatively intense NH–$C^{\beta}H$ correlation in the HOHAHA spectrum. The remaining Ala residue is Ala-1 for which the N-terminal amino group is not observed. Also, a number of Ser (11 of 14), Thr (4 of 6), Val (8 of 11), Ile (3 of 5), and Gly (7 of 8) spin systems could be identified on the basis of the characteristic coupling patterns in the early stages of the assignment process. Ultimately all but a very few of these were completely assigned along with 5 of the 15 Leu and 1 of the 5 Ile residues. Many NH–$C^{\alpha}H$–$C^{\beta}H_2$ spin systems could be attributed to aromatic ring containing residues on the basis of characteristic NOEs between each of these protons and the ring $C^{\delta}H$ group. These include the tyrosine residues for which sequence-specific assignments of the ring spin systems had previously been obtained by a site-directed mutagenesis/^1H NMR study (Gronenborn et al., 1986) and the unique histidine and tryptophan residues, His-30 and Trp-120.

The identification of complete spin systems for proline residues has proved problematic because of the considerable cross-peak overlap in the D_2O spectra. For residues sequential to proline residues, NOEs have been located leading to fragmentary identification of the proline spin systems, specifically the $C^{\alpha}H$ or $C^{\delta}H$ resonances. Complete spin system identification for these and other "long" side chain residues must await the application of 3D ^{13}C–^1H J-correlated spectroscopy (Kay et al., 1990; Bax et al., 1990b).

The complete assignment of the backbone amide NH and non-proline $C^{\alpha}H$ resonances has been made with the aid of the 3D spectra described here. Some assistance was derived from other spectra, including the 3D data sets reported earlier (25 °C and pH 7.5) and a number of 2D spectra recorded under different conditions of pH and temperature. These served mainly to check the assignments as they were made by using the present 3D data sets and also to deal with the small number of residues whose $C^{\alpha}H$ resonance was coincident with the H_2O solvent peak in the 3D data. A summary of the sequential NOE data obtained from the 3D data is given in Figure 8. The NOE data from the 3D NOESY–HMQC experiment described in this paper are represented as a series of black bars. As such, Figure 8 serves to represent the completeness of the NOE connectivity data obtainable from just the single 3D NOESY–HMQC spectrum. The height of the bars is proportional to NOE intensity calculated from the number of contours observed for each peak in the 2D slice of the 3D spectrum for which the NOE appears most intense (on a 0–10 scale, contours are spaced by a factor of 1.5). It is recognized that since each 3D cross-peak is observed in more than a single slice, it is possible that the absolute NOE intensity is slightly underestimated by taking this approach. NOEs that are only observable in 2D spectra recorded in D_2O solution

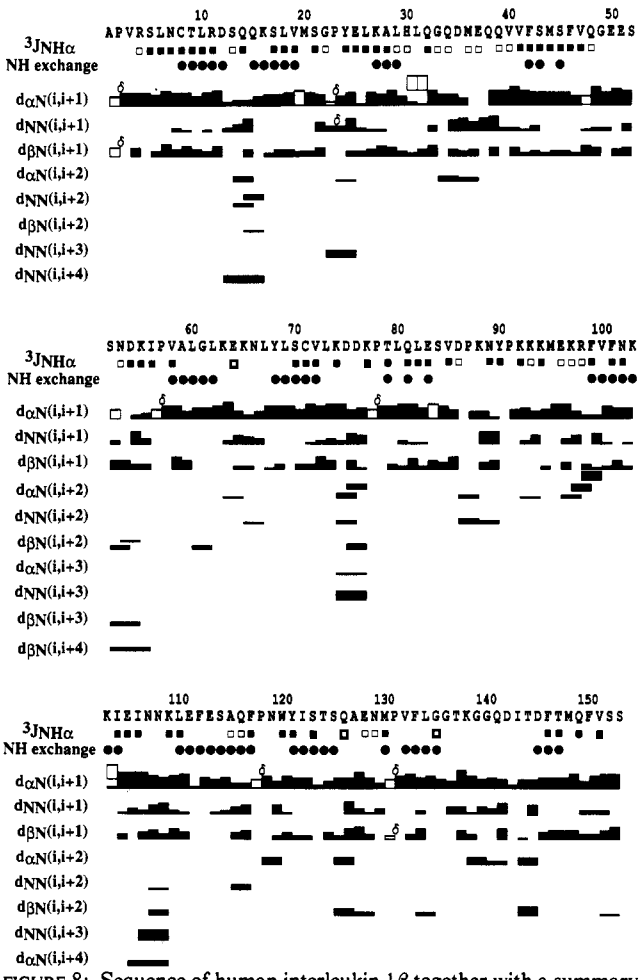

FIGURE 8: Sequence of human interleukin 1β together with a summary of the short-range NOEs involving NH, $C^{\alpha}H$, and $C^{\beta}H$ protons. The NOE intensities are indicated by the black bars and are classified according to the number of contour levels observed for each peak in the 3D NOESY–HMQC spectrum. NOEs that are taken from 2D NOESY spectra are indicated by open bars and are classified as strong, medium, and weak, as indicated by the height of the bars [where both black and open bars are indicated for a given $d_{\alpha N}(i,i+1)$ connection, the NOE in the 3D spectrum is attenuated due to presaturation of the $C^{\alpha}H$ resonance]. A δ indicates that a NOE involves the $C^{\delta}H$ protons of a proline residue in place of an amide NH [i.e., $d_{\alpha P\delta}(i,i+1)$ for $d_{\alpha N}(i,i+1)$, $d_{\beta P\delta}(i,i+1)$ for $d_{\beta N}(i,i+1)$, and $d_{NP\delta}(i,i+1)$ or $d_{P\delta N}(i,i+1)$ for $d_{NN}(i,i+1)$]. Solid circles indicate residues with amide NH resonances that are not fully exchanged 100 min after the protein is dissolved in D_2O at 36 °C and pH 6.1. Residues with accurately measured $^3J_{NH\alpha} > 7.5$ Hz are indicated by solid squares, $^3J_{NH\alpha} < 6.0$ Hz by open squares. The $^3J_{HN\alpha}$ coupling constants were measured from a HMQC–*J* spectrum (Kay & Bax, 1990). The measurements of these NMR parameters are described in a forthcoming paper (Driscoll et al., 1990).

(involving proline $C^{\delta}H$) and NOEs involving those residues whose $C^{\alpha}H$ resonance is wholly or partially obscured by solvent presaturation in the 3D experiment are indicated in Figure 8 by open bars, with their intensities classified as strong, medium, or weak.

Table I lists the ^1H and ^{15}N chemical shifts for both wild-type and des-Ala-1-IL-1β obtained to date. The assignments of the fingerprint region and some NH–$C^{\beta}H$ relayed cross-peaks are indicated in Figure 9, which shows a ^{15}N-decoupled 2D HOHAHA spectrum of ^{15}N-labeled wild-type IL-1β, recorded with a mixing time of 30 ms.

Discussion

The extension of the well-established NMR procedures for sequential assignment, long-range NOE analysis, and coupling constant measurement to molecules of a size greater than 10–12 kDa is fraught with technical difficulties. The most prominent problem is the overall complexity of the spectra of such large molecules. Thus, the chemical shift degeneracy and overlap in the 2D NOESY spectrum of IL-1β is too severe for complete analysis by conventional means (see Figure 1). Concomitant with this is the more fundamental problem of decreasing transverse relaxation times with increasing molecular weight. The consequences of this phenomenon are clearly evident in the 2D HOHAHA spectrum of IL-1β (Figure 1), which shows that the relayed NH–$C^{\beta}H$ connectivities are few and of low intensity. These types of correlations are important for spin system identification and subsequent amino acid type and sequence-specific assignments. To overcome these obstacles, the application of NMR-active isotope-labeling strategies coupled with novel NMR experiments, designed to edit the complex 2D spectra of IL-1β according to the chemical shift of a heteronucleus, can be employed. In particular, there are many examples where uniform ^{15}N labeling has proved useful in the assignment of the ^1H spectra and secondary structure determination of medium-sized proteins, such as Mu *ner* (Gronenborn et al., 1989b) and human thioredoxin (Forman-Kay et al., 1990), through the application of 2D heteronuclear NMR techniques. We have recently reported the application of ^{15}N–^1H 3D heteronuclear NMR to the problem of sequence-specific assignment of the spectrum of IL-1β (Marion et al., 1989b). The basis of the 3D heteronuclear technique is to separate the peaks of the fingerprint region of a 2D ^1H spectrum according to the ^{15}N chemical shift of the amide NH group.

In our previous paper (Marion et al., 1989b) on the application of 3D heteronuclear NMR to IL-1β the sample conditions used were pH 7.5 and 27 °C. These spectra were recorded during a developmental stage of the application of 3D heteronuclear spectroscopy and have not been used extensively in the sequential assignment analysis of IL-1β. The 3D spectra reported in this paper incorporate a number of improvements over those reported previously. These include the optimization of sample conditions to obtain a complete count of amide NH signals and the consecutive recording of the 3D HOHAHA–HMQC and 3D NOESY–HMQC spectra on the same 600-MHz spectrometer.

The sequential assignment of the backbone resonances of IL-1β has been completed with the aid of the heteronuclear 3D spectra described here. We can identify a number of factors that contributed to the success of this approach in this instance. These were as follows:

(1) The 3D spectra almost completely removed the cross-peak overlap problem that was present in the 2D spectra of IL-1β. This factor resulted in a significant simplification of the assignment process, even for cases devoid of chemical shift degeneracy. Consequently, the efficiency of the assignment process was greatly increased.

(2) We were able to unambiguously identify those features of the NOESY spectrum that resulted from the N-terminal heterogeneity of the sample. In the case of resolved amide NH peaks for the two forms of the protein this manifested itself as two different amide strips containing similarly positioned NH–aliphatic NOEs.

(3) That we were able to identify every amide NH and its corresponding $C^{\alpha}H$ proton was of major benefit in the assignment process. In many cases these correlations could be connected unambiguously with sequential NOEs before the spin system identification was confirmed by analysis of the D_2O correlated spectra.

Table I: ^{15}N and ^{1}H Chemical Shifts for Recombinant Wild Type and Human Des-Ala-1-interleukin 1β at pH 5.4 and 36 °C, 100 mM Sodium 1-Acetate-d_3[a]

residue	amide NH		$C^{\alpha}H$	$C^{\beta}H$	other
	^{15}N	^{1}H			
Ala-1			4.17	1.53	
Pro-2			4.50		$C^{\delta}H$ 3.59, 3.68
Val-3	119.1	8.00	4.15	1.93	$C^{\gamma}H_3$ 0.83, 0.83
Arg-4	127.0	8.86	4.46		
	128.3	9.00	4.47		
Ser-5	118.3	8.27	5.67	3.55, 3.68	
	118.4	8.28			
Leu-6	122.4	9.03	4.78	1.82, 1.81	$C^{\gamma}H$ 1.84; $C^{\delta}H_3$ 0.98, 1.02
Asn-7	120.9	8.78	6.25	2.86, 2.32	
Cys-8	117.8	9.59	5.76	2.86, 2.96	
Thr-9	109.5	8.93	5.06	4.39	$C^{\gamma}H_3$ 1.18
Leu-10	120.7	9.41	5.45	1.07, 1.53	$C^{\gamma}H$ 1.18; $C^{\delta}H_3$ 0.58, −0.40
Arg-11	119.6	8.62	5.28	1.60, 1.66	
Asp-12	121.2	8.71	4.65		
Ser-13	114.4	7.42	3.99	3.56, 3.95	
Gln-14	120.4	8.02	4.55	1.59, 2.56	
Gln-15	111.6	8.44	3.71	2.62	
Lys-16	120.2	8.48	3.55	1.97	
Ser-17	119.5	8.27	4.91	4.03, 3.76	
Leu-18	122.4	8.82	5.38	1.40, 2.15	
Val-19	115.5	8.80	4.68	2.03	$C^{\gamma}H_3$ 0.66, 0.78
Met-20	120.9	8.68	4.90	2.19, 1.70	$C^{\gamma}H$ 2.50, 2.36
Ser-21	120.0	8.59	4.52	3.60, 3.52	
Gly-22	111.7	8.11	3.97, 4.12		
Pro-23			4.02		$C^{\delta}H$ 3.59, 3.44
Tyr-24	110.6	8.00	4.78	3.54, 2.76	$C^{\delta}H$ 7.09; $C^{\epsilon}H$ 6.78
Glu-25	119.3	7.20	4.67	1.94, 2.04	$C^{\gamma}H$ 2.24, 2.30
Leu-26	123.0	8.57	5.24	1.63	
Lys-27	119.8	9.18	5.14	1.48, 1.43	
Ala-28	118.9	7.62	6.16	1.31	
Leu-29	125.6	9.42	4.87	1.95, 1.58	
His-30	122.0	10.19	4.69	3.23, 3.16	
Leu-31	126.0	8.40	4.67	1.70, 1.30	
Gln-32	120.2	8.88	4.53	1.98, 2.19	$C^{\gamma}H$ 2.25, 2.31
Gly-33	109.5	8.72	3.77, 3.99		
Gln-34	121.7	8.83	4.27	2.10, 2.10	
Asp-35	119.0	7.86	4.75	2.79, 2.89	
Met-36	118.3	7.68	4.21	2.05	
Glu-37	117.6	8.07	4.22	2.02, 2.10	
Gln-38	117.0	7.94	4.21	1.97, 2.23	
Gln-39	117.3	7.53	4.42		
Val-40	122.7	8.30	3.78	1.58	$C^{\gamma}H_3$ 0.62, 0.19
Val-41	123.9	7.69	4.24	1.83	$C^{\gamma}H_3$ 0.85, 0.85
Phe-42	127.3	9.58	5.04	2.57, 3.07	$C^{\delta}H$ 6.90; $C^{\epsilon}H$ 7.00; $C^{\zeta}H$ 6.62
Ser-43	115.6	9.17	5.16	3.45, 3.61	
Met-44	131.3	9.57	5.30	2.23	
Ser-45	121.1	8.88	5.36	3.58, 3.71	
Phe-46	123.2	8.46	4.77	3.37, 2.98	$C^{\delta}H$ 7.23; $C^{\epsilon}H$ 7.13
Val-47	118.5	7.41	4.66	2.51	$C^{\gamma}H_3$ 0.73, 0.95
	118.6	7.45	4.66		
Gln-48	120.4	8.56	4.44	1.97, 2.08	
	120.5	8.56			
Gly-49	111.6	8.33	3.94, 4.12		
Glu-50	121.3	8.47	4.35	1.92, 2.06	
Glu-51	122.6	8.51	4.50	2.01, 2.09	$C^{\gamma}H$ 2.27, 2.34
Ser-52	116.8	8.39	4.63	3.97, 3.88	
Asn-53	119.7	8.61	4.60	2.90, 2.83	
Asp-54	116.2	8.53	4.59	2.77, 2.77	
Lys-55	118.8	7.60	4.69	1.74, 1.51	
Ile-56	122.7	8.37	4.86	2.09	$C^{\gamma 2}H_3$ 1.16
Pro-57			5.37	2.15, 1.83	$C^{\gamma}H$ 1.86; $C^{\delta}H$ 3.96, 4.00
Val-58	117.8	10.01	5.64	2.08	$C^{\gamma}H_3$ 0.82, 0.73
Ala-59	120.9	8.68	5.42	1.51	
Leu-60	124.3	10.53	4.86	1.51, 0.86	
Gly-61	109.9	8.26	4.15, 2.38		
Leu-62	121.4	8.22	4.46	1.41, 1.34	
Lys-63	126.3	8.16	3.84		
Glu-64	118.6	8.90	3.98	2.24, 2.09	
Lys-65	115.1	7.57	4.48	1.47	
Asn-66	116.2	8.40	4.41	3.14, 3.01	
Leu-67	115.7	6.82	5.34	1.17, 1.42	
Tyr-68	121.5	9.18	4.96	3.08, 2.51	$C^{\delta}H$ 6.88; $C^{\epsilon}H$ 6.51
Leu-69	121.8	8.49	4.84	1.96, 1.66	
Ser-70	115.8	9.17	5.23	3.66, 3.28	
Cys-71	119.5	8.35	5.53	2.86, 2.46	
Val-72	117.0	8.80	4.58	1.99	$C^{\gamma}H_3$ 0.55, 0.71
Leu-73	123.7	8.52	4.17	1.48, 1.36	$C^{\gamma}H$ 1.35; $C^{\delta}H_3$ 0.59, 0.43
Lys-74	126.4	8.20	4.39	1.53, 1.80	
Asp-75	127.5	9.22	4.15	2.66, 2.81	
Asp-76	109.9	8.46	4.07	2.79, 2.86	
Lys-77	119.8	7.71	4.66	1.60, 1.67	

Table I (Continued)

residue	amide NH ^{15}N	amide NH ^{1}H	$C^{\alpha}H$	$C^{\beta}H$	other
Pro-78			3.19		$C^{\delta}H$ 3.07
Thr-79	120.0	8.83	4.58	3.93	$C^{\gamma}H_3$ 1.20
Leu-80	127.1	8.83	5.13	2.00, 1.50	$C^{\gamma}H$ 1.60; $C^{\delta}H_3$ 1.09, 0.75
Gln-81	126.3	9.68	4.98	1.96	
Leu-82	122.0	8.44	5.01	1.83, 1.37	$C^{\gamma}H$ 1.59; $C^{\delta}H_3$ 0.71, 0.72
Glu-83	123.8	9.17	4.63	2.10	
Ser-84	121.2	8.71	5.15	3.90, 3.92	
Val-85	117.3	7.92	4.59	1.52	
Asp-86	122.0	8.04	4.90	2.96, 2.69	
Pro-87					
Lys-88	117.1	8.38	4.20	1.80, 1.73	
Asn-89	114.5	7.78	4.75	2.64, 2.50	
Tyr-90	116.5	7.29	4.19	2.30, 2.50	$C^{\delta}H$ 6.74; $C^{\epsilon}H$ 6.63
	116.7	7.30			
Pro-91			4.25		
Lys-92	116.9	7.22	4.42		
	117.3	7.24	4.41		
Lys-93	119.2	8.29	4.00		
	119.3	8.29			
Lys-94	118.0	7.80	4.59	1.75, 1.51	$C^{\gamma}H$ 1.30, 1.26
Met-95	122.5	7.64	4.23		
Glu-96	122.7	9.14	4.09	2.08, 2.23	$C^{\gamma}H$ 2.72, 2.44
Lys-97	121.5	8.23	3.71	1.71, 1.63	$C^{\gamma}H$ 1.30, 1.24
Arg-98	114.2	7.88	3.91	1.56, 1.49	
Phe-99	116.6	7.84	5.16	3.69, 2.87	$C^{\delta}H$ 7.51; $C^{\epsilon}H$ 7.04; $C^{\zeta}H$ 6.89
Val-100	117.8	7.45	4.36	1.92	$C^{\gamma}H_3$ 0.82, 0.90
Phe-101	127.2	9.83	5.15	2.70, 2.67	$C^{\delta}H$ 6.98; $C^{\epsilon}H$ 7.06; $C^{\zeta}H$ 6.81
Asn-102	121.1	10.38	5.01	2.29, 2.92	
Lys-103	127.7	9.38	4.64		
Ile-104	133.7	9.23	4.45	1.74	$C^{\gamma 2}H_3$ 0.90
Glu-105	126.8	8.48	5.14	1.73, 1.94	$C^{\gamma}H$ 2.05, 2.14
Ile-106	125.6	8.67	4.33	1.68	$C^{\gamma 2}H_3$ 0.80; $C^{\gamma 1}H$ 1.36, 1.03; $C^{\delta}H_3$ 0.78
Asn-107	126.4	9.28	4.27	2.99, 2.72	
Asn-108	110.7	8.81	4.38	3.02, 3.02	
Lys-109	120.1	8.03	4.78	1.85, 1.83	
Leu-110	121.0	9.43	5.42	1.36, 0.94	$C^{\gamma}H$ 1.54; $C^{\delta}H_3$ 0.77, 0.73
Glu-111	117.8	8.76	5.00	1.99	
Phe-112	119.5	10.28	5.23	2.36, 2.54	$C^{\delta}H$ 6.62; $C^{\epsilon}H$ 6.65
Glu-113	126.2	8.82	4.47		
Ser-114	121.9	9.14	3.90	4.37, 4.10	
Ala-115	128.5	8.12	4.05	1.17	
Gln-116	116.9	7.87	3.61	0.98, 1.42	
Phe-117	116.9	7.38	4.86	2.58, 2.64	$C^{\delta}H$ 6.91; $C^{\epsilon}H$ 6.81
Pro-118			4.40	2.29	$C^{\gamma}H$ 3.31, 3.54; $C^{\delta}H$ 1.87, 2.00
Asn-119	114.1	10.23	4.04	3.37, 3.03	
Trp-120	119.7	8.11	4.98	3.67, 2.92	$N^{\epsilon}H$ 10.01; $C^{\delta 1}H$ 7.30, $C^{\zeta 2}H$ 7.45; $C^{\eta 2}H$ 7.21; $C^{\zeta 3}H$ 7.21; $C^{\epsilon 3}H$ 7.10
Tyr-121	119.4	9.40	5.64	2.41, 3.50	$C^{\delta}H$ 7.01; $C^{\epsilon}H$ 6.63
Ile-122	124.6	8.65	3.84	1.62	$C^{\gamma 2}H_3$ 0.41
Ser-123	122.5	8.98	5.82	3.00, 2.06	
Thr-124	109.9	8.99	4.83	4.39	$C^{\gamma}H_3$ 1.16
Ser-125	113.8	9.55	4.97	3.93, 3.98	
Gln-126	122.1	8.87	3.98	2.01, 2.24	$C^{\gamma}H$ 2.38, 2.63
Ala-127	120.0	8.17	4.38	1.44	
Glu-128	117.2	8.44	4.04	2.27, 1.96	
Asn-129	114.1	8.06	4.18	3.31, 2.55	
Met-130	117.7	8.84	5.23	2.15, 2.36	
Pro-131			5.20		$C^{\delta}H$ 3.94, 3.78
Val-132	125.4	8.01	4.42	1.75	$C^{\gamma}H_3$ 0.86, 0.86
Phe-133	124.6	8.65	5.27	3.30, 2.97	$C^{\delta}H$ 7.31; $C^{\epsilon}H$ 7.23; $C^{\zeta}H$ 7.13
Leu-134	119.7	8.58	5.21		
Gly-135	114.9	9.34	4.02, 4.92		
Gly-136	111.2	8.75	2.93, 3.84		
Thr-137	112.1	7.46	4.31	3.99	$C^{\gamma}H_3$ 0.96
Lys-138	124.4	8.37	4.29	1.53, 1.56	
Gly-139	111.5	8.63	3.83, 4.02		
Gly-140	109.0	8.15	3.78, 4.20		
Gln-141	119.7	8.40	4.29	2.00, 2.20	
Asp-142	119.6	7.79	4.93	2.82, 2.57	
Ile-143	125.5	9.18	3.92	2.41	$C^{\gamma 2}H_3$ 0.78
Thr-144	111.8	8.12	4.99	4.39	$C^{\gamma}H_3$ 0.96
Asp-145	120.6	7.10	5.58	2.42, 2.54	
Phe-146	118.0	9.55	5.22	3.09, 2.63	$C^{\delta}H$ 7.01; $C^{\epsilon}H$ 7.11; $C^{\zeta}H$ 6.81
Thr-147	110.0	9.47	4.74	4.19	$C^{\gamma}H_3$ 1.22
Met-148	121.3	8.67	5.39	1.78, 1.78	
Gln-149	123.7	8.43	4.63	2.07	
Phe-150	123.7	8.72	4.77	3.26, 3.03	$C^{\delta}H$ 7.33; $C^{\epsilon}H$ 7.39
Val-151	122.6	8.05	4.36	1.84	$C^{\gamma}H_3$ 0.95, 0.90
Ser-152	119.4	8.39	4.48	3.94, 3.94	
Ser-153	122.5	7.98	4.31	3.89, 3.89	

[a] Where two sets of chemical shifts are given, the second set refers to des-Ala-1-IL-1β. ^{1}H chemical shifts are expressed relative to 4,4-dimethyl-4-silapentane-1-sulfonate, ^{15}N ones relative to external liquid NH_3.

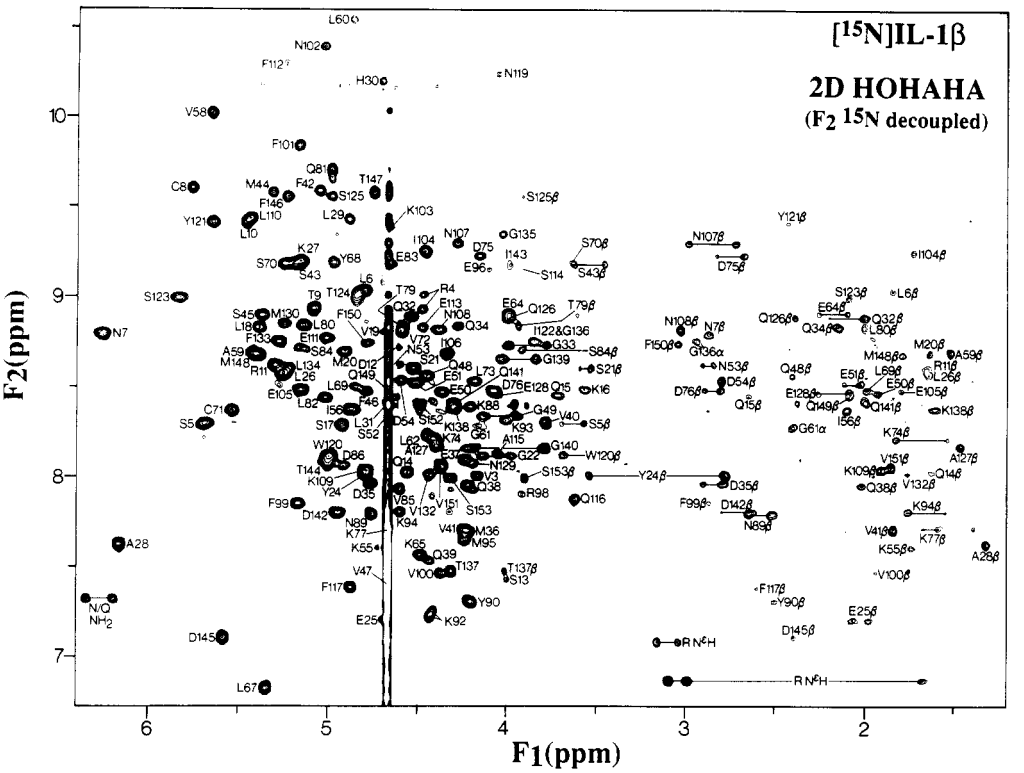

FIGURE 9: NH (F_2 axis)–aliphatic (F_1 axis) region of the 30-ms HOHAHA spectrum of ^{15}N-labeled wild type interleukin 1β in H_2O at 36 °C and pH 5.4. ^{15}N decoupling was applied during t_2 only. The assignments of the NH–C$^{\alpha}$H cross-peaks are indicated, as are those for a number of relayed NH–C$^{\beta}$H cross-peaks. The doubling of NH–C$^{\alpha}$H cross-peaks for residues Arg-4 and Lys-92 is shown. The NH–C$^{\alpha}$H cross-peaks of residues Ser-114 and Lys-63 are not detectable at the contour level chosen.

(4) The sensitivity of the 3D experiment is such that we were able to identify $d_{\alpha N}(i,i+1)$ and $d_{NN}(i,i+1)$ NOE connections between a very large number of pairs of spin systems. The $d_{\alpha N}(i,i+1)$ type of NOE can be observed across almost the entire protein sequence (see Figure 8). (The succeeding residues Met-36, Glu-37, and Gln-38 and Asn-53 and Asp-54 have degenerate C$^{\alpha}$H resonances, and it is impossible to distinguish intra- from interresidue NH–C$^{\alpha}$H NOE intensity in these cases.) Some of the sequential NOE cross-peaks are very weak or absent in the corresponding 2D NOESY spectrum. In this respect we note that, in contrast to the 2D case where resolution enhancement is almost obligatory, the absence of significant overlap in the F_3 dimension of 3D spectrum allows one to apply a digital filtering function to the F_3 time domain data that maximizes sensitivity in the spectrum rather than attempts to improve resolution. (We have not used a strong resolution enhancement function in the F_1 dimension, where resolution of aliphatic CH resonances is relatively poor. Though possible, in principle, to do so would be at the expense of overall signal-to-noise ratio.) In fact, it is possible to trace sequential assignments with either or both $d_{\alpha N}(i,i+1)$ or $d_{NN}(i,i+1)$ NOE connections with no breaks in the interproline segments of the protein sequence.

The ability to separate and identify all the ^{15}N–NH–C$^{\alpha}$H correlations prior to the sequential NOE analysis was of major importance in our success in completing the assignment of IL-1β. This is especially important as it allowed us to use a data reduction approach prior to analysis without the risk of omitting important information. In this regard, the Overbodenhausen ^{15}N–^{1}H correlation experiment is especially suited to the task of "counting" amide NH signals. This is because of the efficient transfer of magnetization from the ^{15}N nucleus to the directly bonded proton. The large scalar coupling for this interaction ($^{1}J_{NH} \sim 90$ Hz) renders this experiment much less sensitive to the short transverse relaxation times of large proteins than ^{1}H–^{1}H correlated experiments. Coupled with the excellent resolution in the ^{15}N dimension, we have found that the ^{15}N–^{1}H Overbodenhausen correlation experiment is able to resolve almost all the amide ^{15}N–^{1}H correlations in the spectrum of IL-1β. What is more, the small degree of cross-peak overlap in this spectrum appears exquisitely sensitive to the sample conditions since *both* the ^{15}N and ^{1}H amide proton chemical shifts are pH and temperature dependent.

It is apparent from the preponderance of $d_{\alpha N}(i,i+1)$ connections in the NOE summary shown in Figure 8 that IL-1β is primarily composed of extended β-strands connected by loops and turns. This result is consistent with both circular dichroism studies (Craig et al., 1987) and the model structure that has been proposed from X-ray crystallographic studies (Priestle et al., 1988). We have found little, if any, evidence that the loss of the N-terminal residue Ala-1 from the structure causes any difference in the protein fold, in spite of the sizeable chemical shift differences that are observed for residues that are far from the N terminus in the protein sequence (e.g., Val-47, Lys-92). According to the crystal structure model of the protein, these residues are close in space to the N-terminal stretch of protein that procedes the first β-strand. One interesting consequence, however, of the loss of Ala-1 from the protein sequence is the concomitant loss of the amide NH resonance of Val-3. The amide NH of this residue is visible in the spectrum of wild-type IL-1β under all conditions that we have explored. This contrasts with the amide NH of Arg-4, which is equally labile to exchange broadening at pH 7.5 and 36 °C in both forms of the protein. We can only speculate at this stage as to the cause of this effect. Apparently, the absence of Ala-1 either causes a structural disruption of the N-terminal part of the protein up to residue Val-3 or leaves the amide NH of Val-3 accessible to solvent. Further investigation of this phenomenon must await the complete assignment of the aliphatic resonances of Pro-2 in both forms

of the protein and possibly the complete structure determination. The results of a preliminary analysis of the secondary structure of IL-1β suggest that the residues Ala-1–Arg-4 are not involved in a regular structure element. We will provide an in-depth consideration of the secondary structure elements of IL-1β in a forthcoming publication (Driscoll et al., 1990).

Table I lists the resonance assignments of all the protons that have been identified to date in the spectrum of IL-1β. For a few residues only the NH and $C^{\alpha}H$ resonances have been unambiguously identified. Confidence in the correctness of the assignment in these cases is derived from many sources. First, the completeness of the backbone resonance assignment indicates that all ambiguities have been resolved self-consistently. Second, an analysis of the secondary structure of IL-1β based on this assignment is, for the most part, consistent with the 3-Å resolution model derived from X-ray crystallographic studies (Driscoll et al., 1990). Third, when the fingerprint regions of a number of point mutant IL-1β proteins (i.e., K27C, C71S, K93A, and K94A) are compared under identical conditions, the chemical shifts are significantly altered only for those residues that are located either close in the amino acid sequence or in the overall tertiary structure (unpublished data). Additionally, all those residues that show significantly different fingerprint region chemical shifts for the two forms of IL-1β present in this study (i.e., wild type and des-Ala-1-IL-1β) are either close to the N terminus of the protein sequence or spatially proximate in the X-ray model. The threonine spin system whose chemical shifts are significantly altered in the mutant K138C (Wingfield et al., 1989) is confirmed as belonging to Thr-137. Last, preliminary studies with amino acid specific ^{15}N labeling (performed subsequent to the completion of the sequential assignment analysis) have provided confirmation of the assignments to amino acid type for all those cross-peaks in the 2D ^{15}N-^{1}H Overbodenhausen experiment attributed to leucine, lysine, and methionine residues (data not shown).

We have shown that the application of ^{15}N-^{1}H 3D heteronuclear NMR is generally applicable to the simplification of the ^{1}H 2D spectra of proteins. It is clear that with a greater degree of ^{15}N and ^{1}H NH and $C^{\alpha}H$ chemical shift degeneracy than is present in the spectrum of IL-1β the 3D ^{15}N-^{1}H heteronuclear NMR experiments may provide a less complete resolution of all ambiguities present in the 2D ^{1}H spectrum. This is likely to be the case for proteins with a high α-helical or nonglobular content. In these cases, judicious use of specific amino acid labeling should resolve the ambiguities remaining in the 3D spectra.

Concluding Remarks

We have demonstrated that it is possible to assign the complete set of backbone resonances of a 153-residue protein, namely, recombinant human IL-1β, with the aid of random ^{15}N isotope labeling and 3D heteronuclear NMR techniques. The application of ^{1}H and ^{15}N–^{1}H 2D NMR techniques to this problem had proved frustratingly inadequate. Once the 3D spectra had been obtained, the assignment of the IL-1β spectrum proceeded relatively quickly. The application of heteronuclear 3D NMR spectroscopy to the assignment of the backbone resonances of proteins with molecular weights greater than 10000 is more efficient than strategies based on amino acid specific isotope labeling as only a single sample is required and relatively few spectra need to be recorded. The assignments obtained here have been used in the study of the protein's secondary structure, as well as investigations into the backbone dynamics of this protein. The ^{15}N resonance assignments have been used directly in the accurate measurement of $^{3}J_{NH\alpha}$ coupling constants and amide NH exchange rates (Driscoll et al., 1990).

To our knowledge, this is the first example of the sequential assignment of the NMR spectrum of a protein that has been obtained by using heteronuclear 3D spectroscopy. The promise of this and other similar studies involving ^{13}C labeling suggests that NMR will soon be applicable to studies of protein conformation in the 15000–25000 molecular weight range.

Acknowledgments

We thank Drs. Ad Bax, Lewis E. Kay, and Mitsuhiko Ikura for many useful discussions. We are grateful to Rolf Tschudin for assistance with the spectrometer hardware.

References

Aue, W. P., Bartholdi, E., & Ernst, R. R. (1976) *J. Chem. Phys. 64*, 2229–2246.

Auron, P. E., Webb, A. C., Rosenwasser, J. J., Mucci, S. F., Rich, A., Wolff, S. M., & Dinarello, C. A. (1984) *Proc. Natl. Acad. Sci. U.S.A. 81*, 7901–7911.

Bax, A., Sklenar, V., Clore, G. M., & Gronenborn, A. M. (1987) *J. Am. Chem. Soc., 109*, 7188–7190.

Bax, A., Ikura, M., Kay, L. E., Torchia, D. A., & Tschudin, R. (1990a) *J. Magn. Reson. 86*, 304–318.

Bax, A., Clore, G. M., Driscoll, P. C., Gronenborn, A. M., Ikura, M., & Kay, L. E. (1990b) *J. Magn. Reson.* (in press).

Bodenhausen, G., & Ruben, D. J. (1980) *Chem. Phys. Lett. 69*, 185–189.

Braunschweiler, L., & Ernst, R. R. (1983) *J. Magn. Reson. 53*, 521–528.

Brown, S. C., Weber, P. L., & Mueller, L. (1987) *J. Magn. Reson. 77*, 166–169.

Buell, G., Schulz, M.-F., Selzer, G., Chollet, A., Movva, R., Semon, D., Escanez, S., & Kawashima, E. (1985) *Nucleic Acids Res. 13*, 1923–1938.

Craig, S., Schmeissner, U., Wingfield, P. T., & Pain, R. H. (1987) *Biochemistry 26*, 3570–3576.

Clore, G. M., & Gronenborn, A. M. (1987) *Protein Eng. 1*, 275–288.

Clore, G. M., & Gronenborn, A. M. (1989) *CRC Crit. Rev. Biochem. Mol. Biol. 24*, 479–564.

Clore, G. M., Bax, A., Wingfield, P. T., & Gronenborn, A. M. (1988) *FEBS Lett. 238*, 17–21.

Davis, D., & Bax, A. (1985) *J. Am. Chem. Soc. 107*, 2820–2821.

Dinarello, C. A. (1984) *Rev. Infect. Dis. 6*, 51–95.

Dinarello, C. A. (1988) *Ann. N. Y. Acad. Sci. 546*, 122–132.

Dower, S. K., Kronheim, S. R., March, C. J., Colon, P. J., Hopp, T. P., Gillis, S., & Urdal, D. L. (1985) *J. Exp. Med. 162*, 501–515.

Driscoll, P. C., Clore, G. M., Beress, L., & Gronenborn, A. M. (1989) *Biochemistry 28*, 2178–2187.

Driscoll, P. C., Gronenborn, A. M., Wingfield, P. T., & Clore, G. M. (1990) *Biochemistry* (in press).

Ernst, R. R., Bodenhausen, G., & Wokaun, A. (1987) *Principles of Nuclear Magnetic Resonance in One and Two Dimensions*, Clarendon Press, Oxford, U.K.

Ferreira, S. H., Lorenzetti, B. B., Bristow, A. F., & Poole, S. (1988) *Nature 334*, 698–700.

Fesik, S. W., & Zuiderweg, E. R. P. (1988) *J. Magn. Reson. 78*, 588–593.

Forman-Kay, J. D., Gronenborn, A. M., Kay, L. E., Wingfield, P. T., & Clore, G. M. (1990) *Biochemistry 29*, 1566–1572.

Fuhlbrigge, R. C., Fine, S. M., Unanue, E. R., & Chaplin, D. D. (1988) *Proc. Natl. Acad. Sci. 85*, 5649–5653.

Gesmar, H., & Led, J. J. (1988) *J. Magn. Reson. 76*, 183–192.
Gronenborn, A. M., Clore, G. M., Schmeissner, U., & Wingfield, P. T. (1986) *Eur. J. Biochem. 161*, 37–43.
Gronenborn, A. M., Wingfield, P. T., Schmeissner, U., & Clore, G. M. (1988) *FEBS Lett. 231*, 135–138.
Gronenborn, A. M., Bax, A., Wingfield, P. T., & Clore, G. M. (1989a) *FEBS Lett. 243*, 93–98.
Gronenborn, A. M., Wingfield, P. T., & Clore, G. M. (1989b) *Biochemistry 28*, 5081–5089.
Jeener, J., Meier, B. H., Bachman, P., & Ernst, R. R. (1979) *J. Chem. Phys. 71*, 4546–4553.
Kay, L. E., & Bax, A. (1990) *J. Magn. Reson. 86*, 110–126.
Kay, L. E., Marion, D., & Bax, A. (1989a) *J. Magn. Reson. 84*, 72–84.
Kay, L. E., Torchia, D. A., & Bax, A. (1989b) *Biochemistry 28*, 8972–8979.
Kay, L. E., Ikura, M., & Bax, A. (1990) *J. Am. Chem. Soc. 112*, 888–889.
Kilian, P. L., Kafka, K. L., Stern, A. S., Woehle, D., Benjamin, W. R., DeChiara, T. M., Gubler, U., Farra, J. J., Mizel, S. B., & Lomedico, P. T. (1986) *J. Immunol. 136*, 4509–4514.
Kostura, M. J., Tocci, M. J., Limjuco, G., Chin, J., Cameron, P., Hillman, A. G., Chartrain, N. A., & Schmidt, J. A. (1989) *Proc. Natl. Acad. Sci. U.S.A. 86*, 5227–5231.
Laue, E. D., Skilling, J., & Staunton, J. (1985) *J. Magn. Reson. 63*, 418–424.
LeMaster, D. M., & Richards, F. M. (1988) *Biochemistry 27*, 142–150.
Lowenthal, J. W., & MacDonald, H. R. (1986) *J. Exp. Med. 164*, 1060–1074.
MacDonald, H. R., Wingfield, P. T., Schmeissner, U., Shaw, A., Clore, G. M., & Gronenborn, A. M. (1986) *FEBS Lett. 290*, 295–298.
Macura, S., Huang, Y., Suter, D., & Ernst, R. R. (1981) *J. Magn. Reson. 43*, 259–281.
March, C. J., Mosley, B., Larsen, A., Cerretti, D. B., Breadt, G., Price, V., Gillis, S., Henney, C. S., Lroheim, S. R., Grabstein, K., Conlon, P. J., Hopp, T. P., & Cosman, D. (1985) *Nature (London) 315*, 641–647.
Marion, D., & Wüthrich, K. (1983) *Biochem. Biophys. Res. Commun. 113*, 967–974.
Marion, D., & Bax, A. (1988) *J. Magn. Reson. 80*, 528–533.
Marion, D., Kay, L. E., Sparks, S. W., Torchia, D. A., & Bax, A. (1989a) *J. Am. Chem. Soc. 111*, 1515–1517.
Marion, D., Driscoll, P. C., Kay, L. E., Wingfield, P. T., Bax, A., Gronenborn, A. M., & Clore, G. M. (1989b) *Biochemistry 28*, 6150–6156.
Matsushima, K., Yodoi, J., Tagaya, Y., & Oppenheim, J. J. (1986) *J. Immunol. 137*, 3183–3188.
McIntosh, L. P., Griffey, R. H., Muchmore, D. C., Nielson, C. P., Redfield, A. G., & Dahlquist, F. W. (1987a) *Proc. Natl. Acad. Sci. U.S.A. 84*, 1244–1248.
McIntosh, L. P., Dahlquist, F. W., & Redfield, A. G. (1987b) *J. Biomol. Struct. Dyn. 5*, 21–34.
Moore, M. A. S. (1989) *Immunol. Res. 8*, 165–175.
Mueller, L. (1987) *J. Magn. Reson. 72*, 191–196.
Norris, K., Norris, F., Christiansen, L., & Fiil, N. (1983) *Nucleic Acids Res. 11*, 5103–5112.
Onozaki, K., Matsushima, K., Aggarwal, B. B., & Oppenheim, J. J. (1985) *J. Immunol. 135*, 3962–3968.
Oppenheim, J. J., Kovacs, E. J., Matsushima, K., & Durum, S. K. (1986) *Immunol. Today 7*, 45–56.
Oschkinat, H., Griesinger, C., Kraulis, P. J., Sørensen, O. W., Ernst, R. R., Gronenborn, A. M., & Clore, G. M. (1988) *Nature (London) 332*, 374–377.
Oschkinat, H., Cieslar, C., Gronenborn, A. M., & Clore, G. M. (1989a) *J. Magn. Reson. 81*, 212–216.
Oschkinat, H., Cieslar, C., Holak, T. A., Clore, G. M., & Gronenborn, A. M. (1989b) *J. Magn. Reson. 83*, 450–472.
Priestle, J. P., Schär, H.-P., & Grutter, M. G. (1988) *EMBO J. 7*, 339–343.
Scapigliatti, G., Ghiara, P., Bartalini, M., Tagliabue, A., & Boraschi, D. (1989) *FEBS Lett. 243*, 394–398.
Shaka, A. J., Barker, P. B., & Freeman, R. (1985) *J. Magn. Reson. 64*, 547–552.
States, D. J., Haberkorn, R. A., & Ruben, D. J. (1982) *J. Magn. Reson. 48*, 286–292.
Stockman, B. J., Westler, W. M., Mooberry, E. S., & Markley, J. L. (1988) *Biochemistry 27*, 136–142.
Torchia, D. A., Sparks, S. W., & Bax, A. (1988a) *J. Am. Chem. Soc. 110*, 2320–2321.
Torchia, D. A., Sparks, S. W., & Bax, A. (1988b) *Biochemistry 27*, 5135–5141.
Torchia, D. A., Sparks, S. W., & Bax, A. (1989) *Biochemistry 28*, 5509–5524.
Vuister, G. W., Boelens, R., & Kaptein, R. (1988) *J. Magn. Reson. 80*, 176–185.
Wingfield, P. T., Payton, M., Tavernier, J., Barnes, M., Shaw, A., Rose, K., Simona, M. G., Demaczuk, S., Williamson, K., & Dayer, J.-M. (1986) *Eur. J. Biochem. 160*, 491–497.
Wingfield, P. T., Payton, M., Graber, P., Rose, K., Dayer, J. M., Shaw, A., & Schmeissner, U. (1987a) *Eur. J. Biochem. 165*, 537–541.
Wingfield, P. T., Mattaliano, R. J., MacDonald, H. R., Craig, S., Clore, G. M., Gronenborn, A. M., & Schmeissner, U. (1987b) *Protein Eng. 1*, 413–417.
Wingfield, P. T., Graber, P., Movva, N. R., Clore, G. M., Gronenborn, A. M., & MacDonald, H. R. (1987c) *FEBS Lett. 215*, 160–164.
Wingfield, P. T., Graber, P., Shaw, A. R., Gronenborn, A. M., Clore, G. M., & McDonald, H. R. (1989) *Eur. J. Biochem. 179*, 565–571.
Wüthrich, K. (1986) *NMR of Proteins and Nucleic Acids*, Wiley, New York.
Zoller, M. J., & Smith, M. (1984) *DNA 3*, 479–488.
Zuiderweg, E. R. P., & Fesik, S. W. (1989) *Biochemistry 28*, 2387–2391.